



Environmental controls of non-growing season carbon dioxide fluxes in boreal and tundra environments

Alex Mavrovic¹⁻²⁻³⁻⁴, Oliver Sonnentag²⁻⁴, Juha Lemmetyinen⁵, Carolina Voigt⁴⁻⁶, Nick Rutter⁷, Paul Mann⁷, Jean-Daniel Sylvain⁸, Alexandre Roy¹⁻²

- 5 ¹ Université du Québec à Trois-Rivières, Trois-Rivières, Québec, G9A 5H7, Canada
² Centre d'Études Nordiques, Québec, Québec, G1V 0A6, Canada
³ Polar Knowledge Canada, Canadian High Arctic Research Station campus, Cambridge Bay, Nunavut, X0B 0C0, Canada
⁴ Université de Montréal, Montréal, Québec, H3T 1J4, Canada
10 ⁵ Finnish Meteorological Institute, Helsinki, FI-00560, Finland
⁶ University of Eastern Finland, Kuopio, 70211, Finland
⁷ Northumbria University, Newcastle upon Tyne, NE1 8ST, UK
⁸ Ministère des Ressources naturelles et des Forêts, Québec, Québec, G1H 6R1, Canada
15 *Correspondence to:* Alex Mavrovic (Alex.Mavrovic@uqtr.ca)

Abstract. The carbon cycle in Arctic-boreal regions (ABR) is an important component of the planetary carbon balance, with growing concerns about the consequences of ABR warming on the global climate system. The greatest uncertainty in annual carbon dioxide (CO₂) budgets exists during the non-growing season, primarily due to challenges with data availability and limited spatial coverage in measurements. The
20 goal of this study was to determine the main environmental controls of non-growing season CO₂ fluxes in ABR over a latitudinal gradient (45°N to 69°N) featuring four different ecosystem types: closed-crown coniferous boreal forest, open-crown coniferous boreal forest, erect-shrub tundra, and prostrate-shrub tundra. CO₂ fluxes calculated using a snowpack diffusion gradient method ($n = 560$) ranged from 0 to 1.05 gC m² day⁻¹. To assess the dominant environmental controls governing CO₂ fluxes, a Random Forest machine
25 learning approach was used. We identified that soil temperature as the main control of non-growing season CO₂ fluxes with 68% of relative model importance, except when soil liquid water occurred during zero-degree Celsius curtain conditions ($T_{\text{soil}} \approx 0^{\circ}\text{C}$ and liquid water coexists with ice in soil pores). Under zero-curtain conditions, liquid water content became the main control of CO₂ fluxes with 87% of relative model importance. We observed exponential regressions between CO₂ fluxes and soil temperature (RMSE = 0.024
30 gC m⁻² day⁻¹) in frozen soils, as well as liquid water content (RMSE = 0.137 gC m⁻² day⁻¹) in zero-curtain conditions. This study is showing the role of several variables on the spatio-temporal variability of CO₂ fluxes in ABR during the non-growing season and highlight that the complex vegetation-snow-soil interactions in northern environments must be considered when studying what drives the spatial variability of soil carbon emission during the non-growing season.

35

Keywords: Arctic-boreal regions, Carbon balance, Carbon dioxide flux, Random forest, Non-growing season, Soil temperature, Soil liquid water content, Snow.



1 Introduction

Carbon stocks and fluxes in the Arctic and boreal biomes (hereafter called Arctic-boreal regions; ABR) constitute large components of the planetary carbon balance (Tarnocai et al., 2009; van Huissteden and Dolman, 2012; Carreiras et al., 2017). ABR store substantial quantities of carbon due to inherently slow decomposition rates, largely attributable to cold temperatures (Ravn et al., 2020). ABR are warming up to four times faster than the rest of the planet with potential feedbacks to the global climate system (Derksen et al., 2019; Rantanen et al., 2022). Although ongoing warming of ABR has the potential to lengthen growing seasons, enhance plant growth and increase above-ground carbon storage (Sturm et al., 2005; McMahon et al., 2010), the growing season vegetation response is variable and complex (Myers-Smith et al., 2020). Warmer air and soil temperatures enhance production and release of carbon dioxide (CO₂) from ecosystem respiration, comprising heterotrophic respiration by microbes decomposing soil organic matter, and autotrophic respiration by above- and belowground plant components (Bond-Lamberty and Thomson, 2010). The release of previously frozen carbon stocks is particularly important in regions undergoing permafrost thaw (ground completely frozen for at least two consecutive years) (Schuur et al., 2015; Natali et al., 2021; Miner et al., 2022). If increases in ecosystem respiration exceed those of photosynthetic CO₂ uptake from enhanced plant growth, ABR may shift from a weak net CO₂ sink to a net CO₂ source, thereby generating a potentially non-negligible, positive feedback to the global climate system (Hayes et al. 2011; Gauthier et al., 2015; Natali et al., 2019; Bruhwiler et al., 2021; Virkkala et al., 2021; Braghieri et al., accepted).

During winter months in ABR, landscapes are generally snow-covered, photosynthesis is considered negligible, and therefore non-growing season CO₂ fluxes derive primarily from soil respiration (Christiansen et al., 2012; Webb et al., 2016). It is expected that complex soil-vegetation-snow interactions will lead to regional and local variability in soil respiration rates across ABR because of relationships between vegetation types, snow cover, soil properties, soil moisture and soil temperature (Gouttevin et al., 2012; Busseau et al., 2017; Loranty et al., 2018; Grünberg et al., 2020; Royer et al., 2021). Higher soil temperatures promote microbial activity and increase CO₂ production from soil organic matter decomposition during the non-growing season (Natali et al., 2019). A snowpack acts as an important thermal insulative layer for the soil during winter, keeping soils warmer than the ambient air (Dominé et al., 2016a). Vegetation affects snow properties by increasing snow depth where wind trapping occurs (Callaghan et al., 2011a; 2011b; Busseau et al., 2017), decreasing snow density and thermal conductivity around shrubs (Gouttevin et al., 2012; Dominé et al., 2015; 2016b), decreasing albedo due to protruding branches (Ménard et al., 2012), and causing earlier spring snowmelt due to vegetation thermal conductivity (Wilcox et al., 2019; Kropp et al., 2022). However, Dominé et al. (2022) showed that shrub branches within the snowpack can contribute to mid-winter soil cooling by conducting temperature through the snowpack. Hence, the complex vegetation-snow-soil interactions in northern environments must be considered when studying what drives the spatial variability of soil carbon emission during the non-growing season. Soil microbial activity can also be limited by lack or saturation of available water, meaning that higher amounts of available soil liquid water (LWC) should allow



75 higher heterotrophic respiration rates by increasing soil microbial activity as long as the soil environment is not anaerobic (Linn and Doran, 1984; Knowles et al., 2015). Anaerobic soil conditions are usually found in fully water saturated soils.

80 High uncertainties in non-growing season ABR CO₂ exchange between the ground surface and atmosphere are in part due to limited data availability because of difficulties in accessing these vast, remote regions and the harsh winter conditions creating technical challenges for CO₂ fluxes measurements (Natali et al., 2019; Virkkala et al., 2022). Methods currently available to measure wintertime CO₂ fluxes include: 1) the eddy covariance technique (Baldocchi et al., 2003), 2) chamber measurements under or above the snowpack (McDowell et al., 2000) and 3) snowpack gradient diffusion methods (Sommerfield et al., 1993).
85 Each of these has their advantages and limitations. The eddy covariance technique (EC) exploits the atmosphere's turbulent nature to estimate net CO₂ fluxes at high temporal resolution without environmental disturbance (Baldocchi et al., 2001; Pastorello et al., 2020). Data gaps are common during the ABR winter since the EC equipment is energy-intensive and prone to failure in low temperatures. In addition, solar power supply systems are limited by low sunlight (Jentsch et al., 2021, Pallandt et al., 2022). Furthermore, the EC
90 equipment is stationary and cover a large footprint (250-3000 m). In contrast, plot-scale chamber techniques for measuring CO₂ fluxes are portable methods with a small footprint (< 1m) (Subke et al., 2021; Maier et al., 2022). Chambers can be used either above the snowpack or directly on the ground. Placing a chamber on the snowpack does not provide a direct measurement of soil CO₂ fluxes due to CO₂ retention and lateral diffusion within snowpacks, generally creating a negative bias and uncertainties linking the snow/atmosphere
95 fluxes to soil fluxes (McDowell et al., 2000; Björkman et al., 2010a; Webb et al., 2016). Chambers can also be placed directly on the ground by excavating the snow cover (Elberling et al., 2007), providing a direct measurement of soil CO₂ fluxes that is, however, prone to a positive bias generated by a tunnel effect due to the snow excavation (McDowell et al., 2000; Björkman et al., 2010). Unavoidable snow cover disturbance also reduces the possibility of revisiting locations for temporal surveys because the soil thermal regime is
100 altered by the snow disturbance. Alternatively, permanent chambers can be installed before the first snowfall, but it disturbs the state of the ground and snow cover around the chamber (Webb et al., 2016). The snowpack diffusion gradient method uses snow porosity and tortuosity to estimate CO₂ fluxes from the gas concentration gradient along a vertical snow profile including ambient air above the snowpack (Sommerfield et al., 1993; Pirk et al., 2016; Kim et al., 2019). In this study, the snowpack diffusion gradient method will
105 be used to evaluate the spatial variability of CO₂ fluxes in ABR because of its portability and minimal environmental disturbance.

The goal of this study was to determine the main environmental controls of non-growing season CO₂ fluxes in ABR. 560 snowpack diffusion gradient measurements were made over a latitudinal gradient of four
110 different ecosystem types common in ABR in Canada: closed-crown coniferous boreal forest, open-crown coniferous boreal forest, erect-shrub tundra and prostrate-shrub tundra. Spatio-temporal measurements of snowpack CO₂ diffusion gradients were performed at several locations in four sites during the 2020-2021

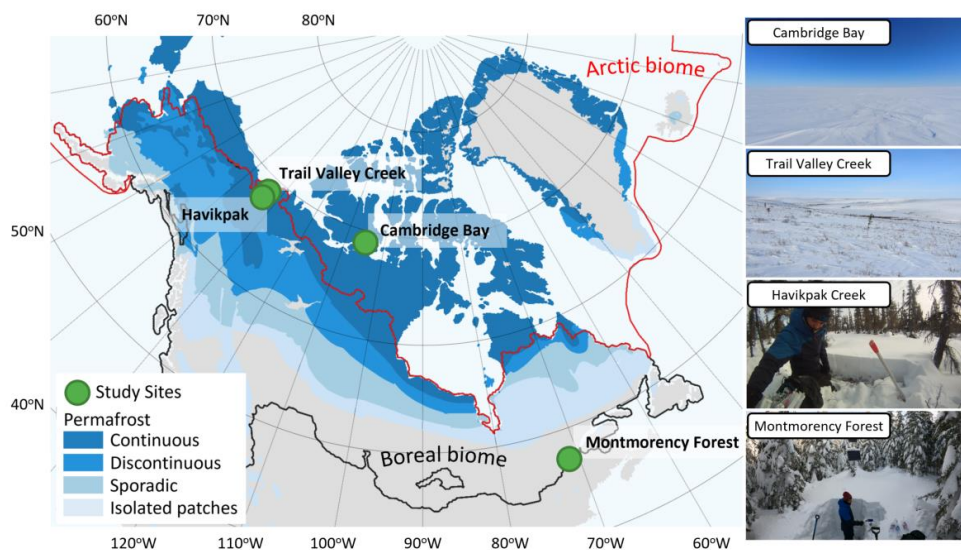


and 2021-2022 winters (December to May). Firstly, a Random Forest (RF) machine learning analysis was used to evaluate the relative importance of the following environmental variables known to exert control over non-growing season CO₂ fluxes: soil temperature, soil LWC, vegetation type, snow water equivalent, snow depth and several snow density-related measurements. Secondly, the response and uncertainty of non-growing season CO₂ fluxes to the most impactful environment variables determined by the RF model were quantified through regression analysis.

2 Method

2.1 Study sites

To cover different vegetation types and a wide range of soil temperature (T_{soil}) regimes and snow conditions found in ABR, four study sites were selected across Canada (Fig. 1; Table 1). Each site represents a specific ecosystem type (Royer et al., 2021), and vegetation types within each of those ecosystems were determined using vegetation maps specific to each site. Cambridge Bay (CB), situated on the Victoria Island in the Canadian Archipelago was the northernmost site located in the Arctic tundra dominated by lichen and prostrate-shrub tundra. Ponomarenko et al. (2019) generated a detailed ecotype map of the Arctic tundra biome present in the CB study area. Here, these ecotypes were grouped by water availability into three tundra vegetation types from which the sampling locations (S) were selected: dry (S=94), sub-hydric (S=24) and hydric (S=110). Trail Valley Creek (TVC), NWT, situated just north of the treeline in the transitional zone between the boreal and Arctic biomes close to the Mackenzie delta, is dominated by erect-shrub tundra with remaining tree patches (Martin et al., 2022). Grünberg et al. (2020) produced a vegetation map of the TVC study area using airborne orthophotos, vegetation height and field observations from which seven vegetation types and landforms were identified: lichen (S=68), tussock (S=21), dwarf shrub (S=19), tall shrub (S=26), polygon (S=21), riparian shrub (S=17) and black spruce tree patch (S=18). Havikpak Creek (HPC) is located just south of the treeline, at about 50 km south of TVC in an open-crown black spruce dominated forest constituting the only type of vegetation present (S=30) (Krogh et al., 2017). Montmorency Forest (MM) is the southernmost site located in a closed-crown balsam fir dominated boreal forest constituting the only type of vegetation present (S=110) (Barry et al., 1988). The CB, TVC and HPC sites are underlain by continuous permafrost, while the MM site is permafrost-free.



140

Figure 1: Study site locations in Canada. The Arctic biome is delimited following the Conservation of Arctic Flora and Fauna (CAFF) working group of the Arctic Council and the boreal biome is delimited following Potapov et al. (2008). Permafrost extent (Brown et al., 2002) is estimated in percent area: continuous (>90-100%), discontinuous (>50-90%), sporadic (10-50%) and isolated patches (<10%).

145

Table 1: Study sites with the number of sampling locations in Canada and CO₂ flux measurement (N) for each site.

Site	Province/ Territory	Latitude/ longitude	Ecosystem	Sampling locations	N	Measurement Dates (YYYY-MM)	Site reference
Cambridge Bay	Nunavut	69°13'N 104°54'W	Prostrate tundra shrubs	47	230	2021-04, 12 2022-01 to 05	Ponomarenko et al., 2019
Trail Valley Creek	Northwest Territories	68°46'N 133°28'W	Erect tundra shrubs	34	190	2021-03, 12 2022-03	Grünberg et al., 2020
Havikpak Creek	Northwest Territories	68°19'N 133°31'W	Open-crown coniferous boreal forest (black spruce)	5	30	2021-03, 04 2022-03	Krogh et al., 2017
Montmorency Forest	Quebec	47°18'N 71°10'W	Closed-crown coniferous boreal forest (balsam fir)	12	110	2021-01, 02, 12 2022-01 to 05	Barry et al., 1988

2.2 Snowpack diffusion gradient method

150 2.2.1 CO₂ flux calculation

During the non-growing season in ABR, soil respiration produces CO₂ below the snowpack. Consequently, a vertical CO₂ diffusion gradient is maintained through the snowpack ($d[\text{CO}_2]/dz$; gC m^{-4}) (Jones et al., 1999). The snowpack diffusion gradient method uses the $d[\text{CO}_2]/dz$ within the snowpack and Fick's first law for gas diffusion through porous media to estimate CO₂ fluxes (F_{CO_2} ; $\text{gC m}^{-2} \text{day}^{-1}$) (Sommerfeld et al., 1993; Zhu et al., 2014):

155



$$F_{CO_2} = -\varphi\tau D \frac{d[CO_2]}{dz} \quad (1)$$

where φ represents the porosity of the snow medium, τ its tortuosity and D the diffusion coefficient of the diffused gas in $m^2 \text{ day}^{-1}$. The porosity of dry snow can be assessed from its density (Kinar and Pomeroy, 2015):

$$\varphi = 1 - \frac{\rho_{snow}}{\rho_{ice}} \quad (2)$$

where ρ represents the density of snow and pure ice ($\rho_{ice} = -0.0001 \cdot T_{ice} + 0.9168$ with T_{ice} as ice temperature in $^{\circ}\text{C}$ and ρ_{ice} in g cm^{-3} ; Harvey et al., 2017). The tortuosity is strongly correlated with porosity. Prieur du Plessis and Masliyah (1991) established the following relationship:

$$\tau = \frac{1 - (1 - \varphi)^{2/3}}{\varphi} \quad (3)$$

Tortuosity can also be approximated as $\tau \approx \varphi^{1/3}$ (Millington, 1959; Mast et al., 1998). The $d[CO_2]/dz$ is obtained by measuring the $[CO_2]$ vertical profile at various snow depths. Standard diffusion coefficients of CO_2 are available in literature but must be corrected for temperature and pressure (Marrero and Mason, 1972; Massman, 1988):

$$D = 0.2020 \cdot \left(\frac{T}{T_o}\right)^{1.590} \cdot e^{-\frac{0.3738}{T/T_o}} \quad (4)$$

where T is the air temperature and T_o is the freezing point in K. The diffusion gradient method assumes that gas fluxes are the result of simple, linear, gradient-induced diffusion in uniform porosity through snow cover (McDowell et al., 2000). A snowpack with strongly heterogeneous density (i.e., vertical stratification) can induce a bias when gas flow is altered by dense layers or ice crusts, typically leading to F_{CO_2} overestimation (Seok et al., 2009). Such layers were rarely found in our study sites. The diffusion gradient assumption also does not hold when strong wind events occur, decreasing snowpack CO_2 concentration through wind-pumping and inducing a negative bias on CO_2 fluxes (Seok et al., 2009). Consequently, $d[CO_2]/dz$ was not measured in days following a strong wind event.

2.2.2 Data collection

All data were collected during the 2020-21 and 2021-22 winters between December and May (Table 1). The CO_2 concentration gradient was measured by collecting gas samples at various depths in the snowpack.



Each gradient profile consisted of five gas samples collected at: 1) 5 cm above the snowpack (ambient air),
190 2) 5 cm depth below the snowpack surface, 3) 1/3 of total snow depth, 4) 2/3 of total snow depth and 5)
soil/snow interface. Gas present in snow pores was collected with a hollow, thin stainless-steel rod (50-120
cm long, 4 mm outer diameter and 2 mm inner diameter) to minimize snow disturbance (Fig. 2a). Gas was
collected in a 60 mL syringe (Air-Tite Luer Lock, Virginia Beach, Virginia) connected to the rod via a three-
way valve. Gases were transferred into 12 mL hermetic glass vials (Labco Exetainer®, Labco Ltd., Lampeter,
195 UK), which were sent to the Université du Québec à Trois-Rivières laboratory to be measured with a gas
analyzer to obtain CO₂ concentrations. At each site, several sampling locations were selected to cover the
maximum range of vegetation types and snowpack characteristics, covering areas of 0.05-22.5 km². At each
sampling location, 2 to 4 replicate profiles were measured at 50 cm spacing to test the repeatability of the
sampling. A minimal spacing of 5 – 7.5 cm was required between sampling positions since it corresponds to
200 the radius of the 60 ml sampling volume of each gas sample, based on a snow density range of 100 - 650 kg
m⁻³.

For typical Arctic snowpacks, samples at 1/3 depth are usually in wind slab, the dense and cohesive
surface snow layer formed by strong Arctic winds. Samples at 2/3 depth are usually in depth hoar, the lower
205 snow layer with low density and cohesion formed by a strong temperature gradient driving vertical vapor
flux through the snowpack (Fig. 2b). Typically, boreal snowpacks are deeper than in Arctic tundra and display
a more continuous vertical stratification with increasing snow density at the bottom of the snowpack. In HPC,
snowpack depths were 40-80 cm in March, while snowpack depths at MM were 100-200 cm (Fig. A1). For
comparison, by March, snowpacks at CB were 10-75 cm deep and 15-150 cm at TVC.

210

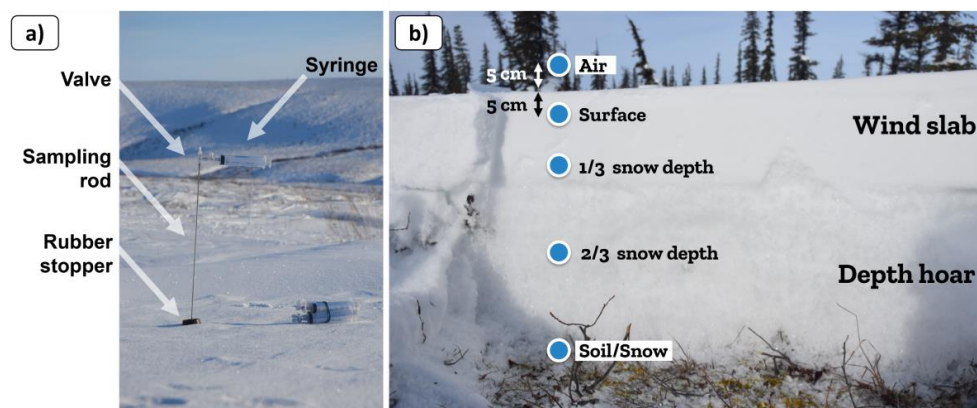


Figure 2: (a) Gas sampling equipment for the CO₂ concentration gradient measurement. (b) Typical snow depth profile of an Arctic snowpack (picture from Trail Valley Creek close to a tree patch).

215 Once the gas samples were collected, a vertical profile of snow and soil properties was measured to
calculate snow porosity, tortuosity and the CO₂ diffusion coefficient. Snow properties included snow and soil



temperature (Snowmetrics digital thermometer; Fort Collins, Colorado; tenth of a degree resolution), snow density (Snowmetrics digital scale, 100 and 250 cm³ snow cutters; $\sigma(\rho_{\text{snow}}) \approx 9\%$; Proksch et al., 2016) and snow stratigraphy. T_{soil} was measured at 1 cm depth under the soil/snow interface, three measurements of T_{soil} were averaged. Snow depth measurements were done with a ruler graduated every 1cm ($\sigma(d_{\text{snow}}) \approx 0.5\text{cm}$).

The CO₂ concentration of 86% of gas samples were measured using a Licor LI-7810 CH₄/CO₂/H₂O Trace Gas Analyzer (LI-COR Biosciences, Lincoln, Nebraska; $\sigma < 1\%$; N = 483). The gas samples were passed through an open loop along a continuous flow of a 200 ppm CO₂ calibration gas (Linde Canada, Ottawa, Ontario, Canada). Based on a calibration curve using 0, 400 and 1000 ppm CO₂ calibration gases (Linde Canada), the CO₂ concentration of gas samples were calculated (detailed protocol: <https://www.licor.com/documents/xst0ld9jozfb78bmqdqi9i7rmjjjmg>).

Randomly distributed gas samples collected during the 2020-21 winter were analyzed with a Picarro G2201-I CRDS gas analyzer (Picarro, Santa Clara, California; $\sigma < 0.1\%$; N = 26). CO₂ concentrations estimated from the LI-7810 and Picarro gas analyzers were not significantly different in their concentration range and distribution (Fig. A2; $R^2 = 0.92$). At TVC in March 2022, a portable LI-850 CO₂/H₂O Gas Analyzer was used ($\sigma < 1.5\%$; N = 38), allowing for CO₂ concentrations to be measured on the same day as sample collection (avoiding the need for bottling and transportation). CO₂ concentrations estimated from the LI-7810 and LI-850 gas analyzers were not significantly different in their concentration range and distribution (Fig. A2b; $R^2 = 0.82$).

2.2.3 Evaluation of CO₂ flux uncertainties

An uncertainty assessment was conducted to evaluate CO₂ flux precision based on the snowpack diffusion gradient method. From sampling to flux estimation, several steps could add uncertainty to the results. Uncertainties can be subdivided into four sources: gas concentration estimates, gas transfer/transport/storage, evaluation of the snowpack $d[\text{CO}_2]/dz$ and snowpit measurements. Gas concentration uncertainties were evaluated from the gas analyzer precision as assessed by the manufacturer and testing using calibration gases. Six CO₂ reference gases of 400 ppm were bottled during two different field campaigns and were processed among the gas samples from the snowpack to ensure the transfer, transport and storage protocol did not lead to sample contamination. The $d[\text{CO}_2]/dz$ uncertainties were evaluated with the standard deviation from the coefficient of determination ($\sigma = \sqrt{(1 - R^2)/(N - 1)}$; Bowley, 1928). Using $d[\text{CO}_2]/dz$ and snow density uncertainties, F_{CO_2} uncertainties were calculated with the min-max uncertainty propagation method.



250 2.3 Soil volumetric liquid water content at Montmorency Forest site

When the soil is under zero-degree Celsius curtain conditions, the soil temperature is around freezing point (0°C) and a mix of ice and liquid water coexists in the soil pore space because the phase transition between water and ice is slowed due to latent heat (Outcalt et al., 1990). Hence, liquid water content (LWC; m³/m³) and ice fractions can be used as a freezing/thawing indicator during the zero-curtain period.

255 The MM study sites were equipped with TEROS 12 Soil Moisture Sensors (METER Group) at 5 cm depth. LWC was only monitored at the MM site since it was the only site where the T_{soil} measurements indicates that the zero-curtain was maintained throughout the winter season, allowing liquid water in the soil throughout the winter. The Zhang et al. (2010) empirical soil liquid water and ice mixing model was used to calculate soil liquid water content (m_{uw}) and ice fraction from permittivity probes:

260

$$LWC = a \cdot \frac{\rho_b}{\rho_w} \cdot |T_{soil}|^{-b} \quad (5)$$

$$\ln a = 0.5519 \cdot \ln SSA + 0.2618 \quad ; \quad \ln b = -0.264 \cdot \ln SSA + 0.3711 \quad (6)$$

where ρ_w and ρ_b (g cm⁻³) represent liquid water and soil bulk density respectively, T_{soil} (°C) represents soil temperature, SSA (m⁻¹) represents soil particles specific surface area described by Fooladman (2011).

265

$$SAA = 3.89 \cdot d_g^{-0.905} \quad (7)$$

$$\ln d_g = f_c \cdot \ln M_c + f_{si} \cdot \ln M_{si} + f_{sa} \cdot \ln M_{sa} \quad (8)$$

270

where d_g represents the soil geometric mean particle-size diameter (mm), f and M represent soil fraction and mean particle-size diameter of soil components (mm). Soil components are clay ($M_c = 0.001$ mm), silt ($M_{si} = 0.026$ mm) and sand ($M_{sa} = 1.025$ mm). Soil bulk density and gravimetry was evaluated using a soil sampling protocol similar to the National Forest inventory protocol (CFI, 2008). Undisturbed soil samples were collected in three homogenous horizons of a soil profile using 400 cm² cores. Volumetric soil samples were dried (103°C) and weighted to determine bulk density. Gravimetric samples were used to determine sand (%), 50-2000 μm), silt (%), 2-50 μm), clay (%), < 2 μm) and organic content (g/kg). The soil texture was determined by the hydrometer method (Bouyoucos, 1962), whereas the organic content was determined with a LECO organic analysis instrument (LECO corporation, Saint-Joseph, Michigan).

275

280 2.4 Random Forest algorithm

Random forest (RF) is an ensemble machine learning method based on a decision trees (Breiman, 2001). Each decision tree of our RF model (scikit-learn 1.2.1 library from python 3.10.3) is trained on a random subset of environmental variables drawn from the dataset input: T_{soil}, LWC, vegetation type, snow

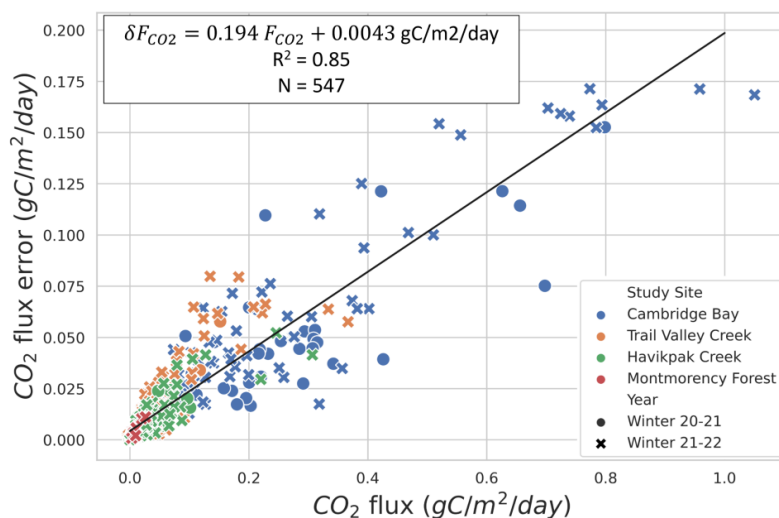


285 water equivalent, snow depth, snow mean density, snow maximum density, snow porosity, snow tortuosity,
wind slab thickness (if present) and wind slab fraction relative to total snow depth (if present). Each decision
tree generates a F_{CO_2} prediction, and the overall RF prediction is the average of all prediction trees. A strength
of the RF algorithm is that it performs well even when input variables are correlated with each other (Liaw
and Wiener, 2002; Strobl et al., 2008; Kibtia et al., 2020). Our RF model was composed of 500 fully
decomposed decision trees. Our dataset was randomly divided into a training subset (75%) and a testing
subset (25%), preserving the relative distribution between vegetation types. Our RF model performance was
290 assessed using the coefficient of determination (R^2), explained variance, and mean absolute error. We used
our RF model to identify the relative importance of non-growing season CO_2 flux predictors. Relative
importance of each environmental variable was computed with the permutation method, i.e., alternatively
removing variables from the RF model and evaluating the performance decrease which was, measured via
295 the coefficient of determination.

3 Results

3.1 CO_2 flux uncertainties

Evaluation of F_{CO_2} precision showed that two main sources of uncertainty are associated with snow
density measurements, in agreement with Sommerfeld et al. (1996), and with $d[CO_2]/dz$ linear regression
300 (mean $R^2 = 0.790$ ($\sigma = 0.236$) for $F_{CO_2} \geq 0.01$ $gC\ m^{-2}\ day^{-1}$; $N = 398$) (Table A1). Snow density uncertainty
($\sigma(\rho_{snow}) \approx 9\%$) impacted snow porosity and tortuosity in Eq. 1. From the linear fit of Fig. 3, the average F_{CO_2}
uncertainty can be estimated at 19.4%, which provides sufficient accuracy to observe the impact of
environmental variables on non-growing season F_{CO_2} .



305 **Figure 3:** CO_2 flux (F_{CO_2}) uncertainty relationship to F_{CO_2} for the four study sites and two winter seasons 2020-2021 and 2021-2022. Specifications of the linear fit can be found in the upper left.



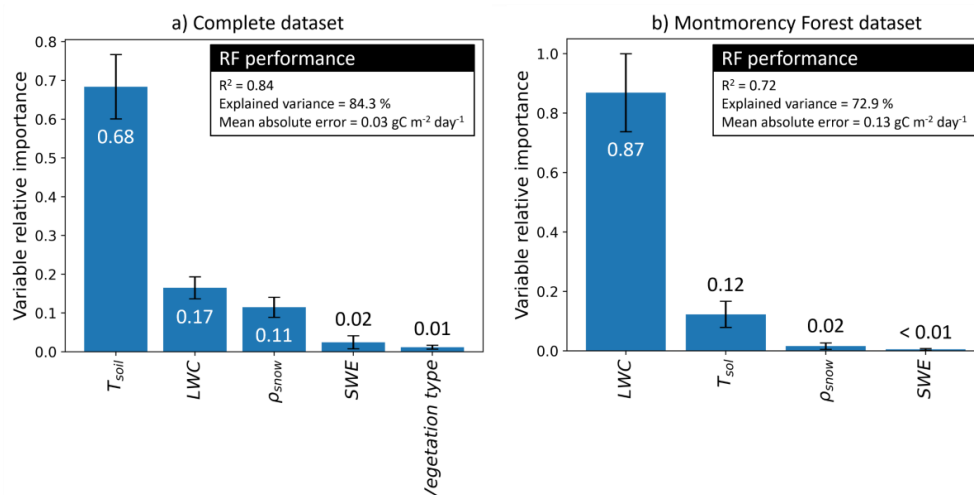
The overall [CO₂] precision of around 1% shows that the measurement technique is not a main source of uncertainty in F_{CO₂} estimates. Gas concentration estimations from LI-7810 have a precision of 0.88% at 400 ppm according to the manufacturer. The stability of the [CO₂] measurement was evaluated over 169 measurements displaying a standard deviation of 0.09%. The LI-7810 was further tested using a 400 ppm calibration gas with a 1% [CO₂] precision (Linde Canada). A linear calibration fit equation was used to estimate [CO₂] of small gas samples, using 3 calibration gases (200, 400, 1000 ppm) plus the theoretical zero intercept. Average uncertainty of the linear regression was 0.76% over six calibration runs with a standard deviation of 0.15%. The average accuracy of the reference [CO₂] bottled among the gas samples from the snowpack was 1.11%.

3.2 Spatio-temporal variability of non-growing season CO₂ fluxes associated with abiotic controls

The RF model determined T_{soil} and LWC were the two main predictors of non-growing season CO₂ fluxes. We found two temperature and LWC regimes of non-growing season F_{CO₂} (Fig. 4). The first regime was when the soil was frozen with T_{soil} < 0°C and LWC < 0.2 m³/m³ leading to F_{CO₂} being mainly controlled by T_{soil}. The second regime was when LWC > 0.2 m³/m³ and < 0.42 m³/m³ but with a fraction of it's water in the form of ice (zero curtain condition), causing LWC to be the main control of F_{CO₂} instead of T_{soil}. Subsequent evaluation focused on the response of non-growing season CO₂ fluxes to T_{soil} and LWC using exponential regressions in order to better understand the role of these two variables on non-growing season CO₂ fluxes.

3.2.1 Variable importance determined by Random Forest model

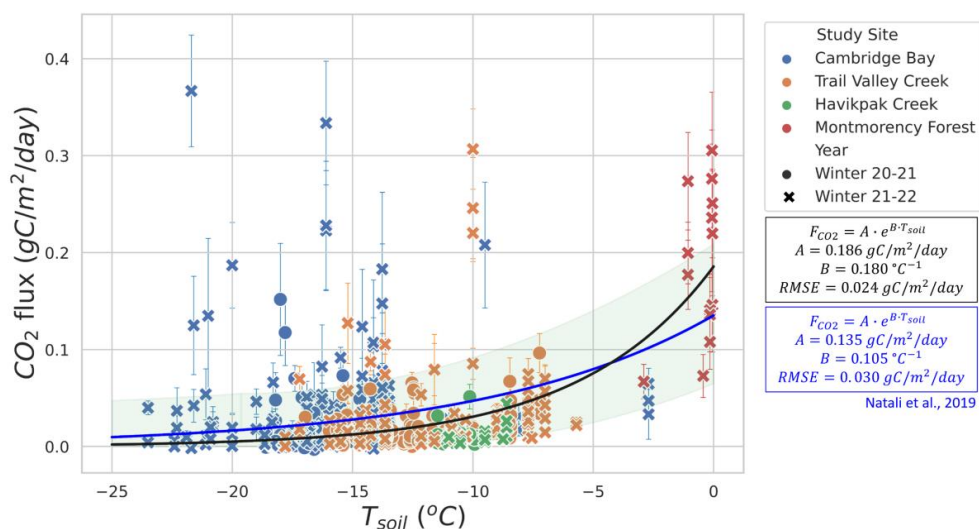
T_{soil} was the F_{CO₂} predictor with the highest relative importance (68%) when using the complete dataset (Fig. 4a), followed by LWC (17%). Snowpack characteristics, ρ_{snow} (11%) and SWE (2%), had a lower relative importance in the RF model. Contrary to what might be expected, the vegetation type had near-negligible relative importance (1%) in F_{CO₂} prediction. The RF model was developed starting with all environmental variables available: T_{soil}, LWC, vegetation type, snow water equivalent (SWE), snow depth, mean ρ_{snow}, max ρ_{snow}, φ, τ, wind slab fraction and wind slab thickness. Although the correlation of several snow parameters did not decrease the RF model performance, snow parameters impacted the assessment of variable relative importance by splitting the relative importance between the correlated variables. Consequently, variables with lower importance and with no significant impacts on the RF performance were progressively removed. The two selected snow parameters that had significant impact were SWE and ρ_{snow}. MM was the only site where soil LWC was present, enabling the assessment of the relative importance of this variable. When using only data from MM in the RF model (Fig. 4b), the relative importance of T_{soil} (12%) on F_{CO₂} was lower than with all combined datasets since T_{soil} was near 0°C for all measurements. At MM, LWC becomes the main predictor (87%) of F_{CO₂}, while ρ_{snow} importance drops (2%) and SWE remains similar (< 1%).



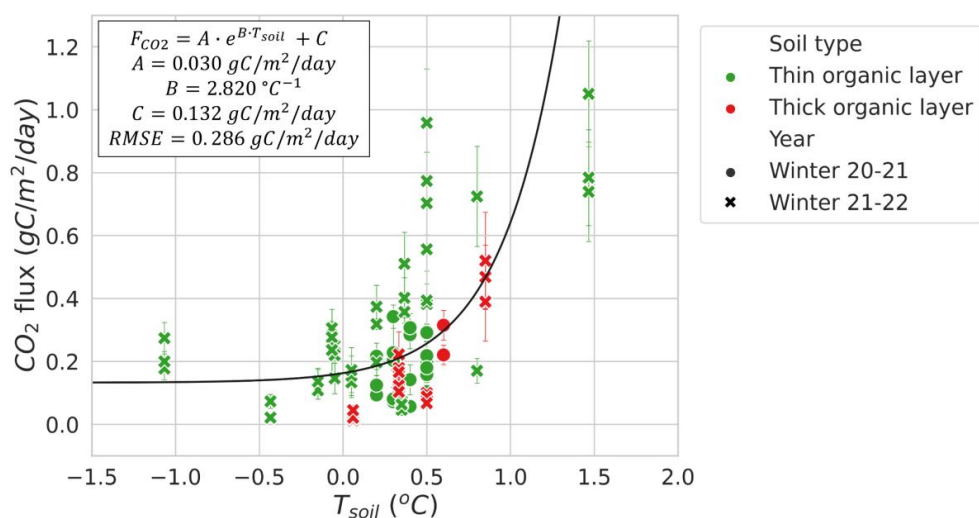
345 **Figure 4:** Random Forest (RF) performance and variable relative importance. Variables used are soil temperature (T_{soil}),
soil liquid water content (LWC), snow density (ρ_{snow}), snow water equivalent (SWE) and vegetation type. (a) The first
iteration integrated the complete dataset and (b) the second iteration only integrated Montmorency Forest dataset with
LWC > 0 m³ m⁻³. The values displayed by the bar plot is the mean variable relative importance over 100 permutations,
while the error bars are the standard deviation.

3.2.2 Soil temperature

350 Figures 5 and 6 show the relationship between non-growing season F_{CO_2} and T_{soil} . Figure 5 focuses on
 $T_{soil} < 0^\circ C$ from CB, TVC, HPC and MM. An exponential regression was used to evaluate the relationship
between T_{soil} and F_{CO_2} estimates (RMSE = 0.024 gC m⁻² day⁻¹). F_{CO_2} at MM when $T_{soil} < 0^\circ C$ and LWC < 0.2
m³/m³ were included in this graph because they are more strongly correlated to T_{soil} than LWC (see Sect.
3.2.3). Note that the lack of F_{CO_2} measurements with T_{soil} between $-6^\circ C$ to $-0.5^\circ C$ restrict the capacity to
355 evaluate the regression within this range. Using the exponential regression of Natali et al. (2019), we obtained
a RMSE of 0.030 gC m⁻² day⁻¹, higher than the one obtained with our dataset. The regression of Natali et al.
(2019) generally shows an overestimation of fluxes for $T_{soil} < -5^\circ C$, but an underestimation for $T_{soil} > 5^\circ C$
when compared to our exponential regression. The systematic bias between our dataset and the regression of
Natali et al. (2019) is minimal (mean bias = -0.0025 gC day⁻¹ m⁻²). We also observed the isolated occurrence
360 of comparably large, non-growing season F_{CO_2} up to 0.36 gC m⁻² day⁻¹ at temperatures below $-10^\circ C$ (Fig. 5).
These measurements of high F_{CO_2} at low temperature seems to be genuine since the repeatability was verified
over the 3 sampling profiles performed at each site. Nevertheless, we were not able to explain these strong
 F_{CO_2} fluxes and no environmental variables measured in our study could be linked to those occurrences.
Figure 6 displays the higher non-growing season F_{CO_2} from MM where T_{air} are higher and the important
365 snowpack insulation keeps the soil at temperatures around $0^\circ C$ through the entire non-growing season. F_{CO_2}
increases rapidly with T_{soil} above the freezing point, which is depicted in the exponential regression (RMSE
= 0.286 gC m⁻² day⁻¹).



370 **Figure 5:** CO₂ flux (F_{CO_2}) as a function of surface soil temperature (T_{soil}) for $T_{soil} < 0^\circ\text{C}$. An exponential regression was fitted with the data (black line) and compared to the exponential regression by Natali et al. 2019 from an external dataset (blue line).



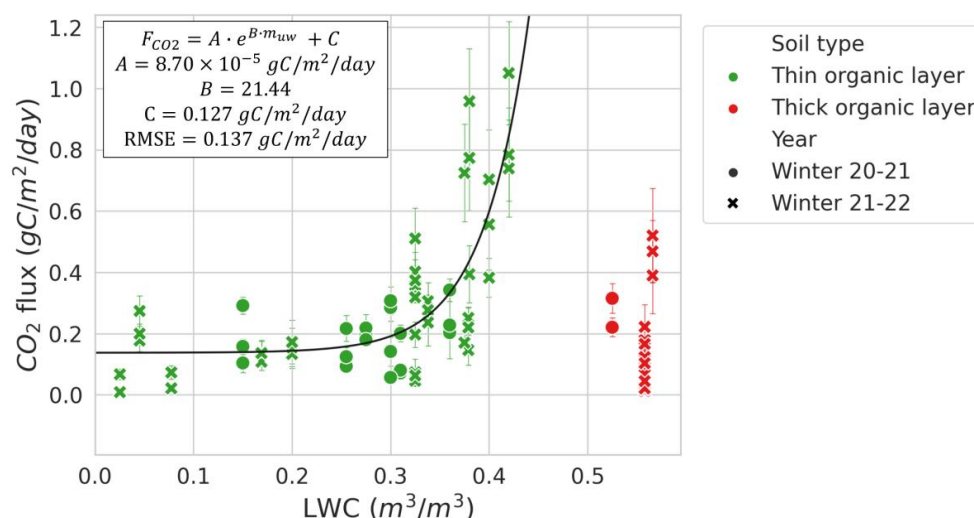
375 **Figure 6:** CO₂ flux (F_{CO_2}) as a function of soil temperature (T_{soil}) at the Montmorency Forest study sites where soil liquid water content (LWC) was greater than $0 \text{ m}^3/\text{m}^3$ through the winter. An exponential regression was fitted to the data (black line).

3.2.3 Soil liquid water content

380 The relationship between LWC and F_{CO_2} during the non-growing season at MM (RMSE = $0.137 \text{ gC m}^{-2} \text{ day}^{-1}$) was stronger than between T_{soil} and F_{CO_2} (RMSE = $0.286 \text{ gC m}^{-2} \text{ day}^{-1}$), when excluding the



sampling location that contained a thick organic soil layer with very high soil moisture due to its location near the bottom of a microtopographic depression (Fig. 7). Other MM sampling locations with a thin organic layer shared a similar soil compositions dominated by mineral soils. The strong correlation between LWC and F_{CO_2} was mostly observed at $LWC > 0.2 \text{ m}^3/\text{m}^3$ and $< 0.42 \text{ m}^3/\text{m}^3$. The plateau observed in Fig. 7 indicates that T_{soil} might be a better predictor than LWC at $LWC < 0.2 \text{ m}^3/\text{m}^3$.



390 **Figure 7:** CO_2 flux (F_{CO_2}) as a function of soil volumetric liquid water content (LWC) at the Montmorency Forest study sites. An exponential regression was fitted to the data (black line), excluding the thick organic layer site (red markers).

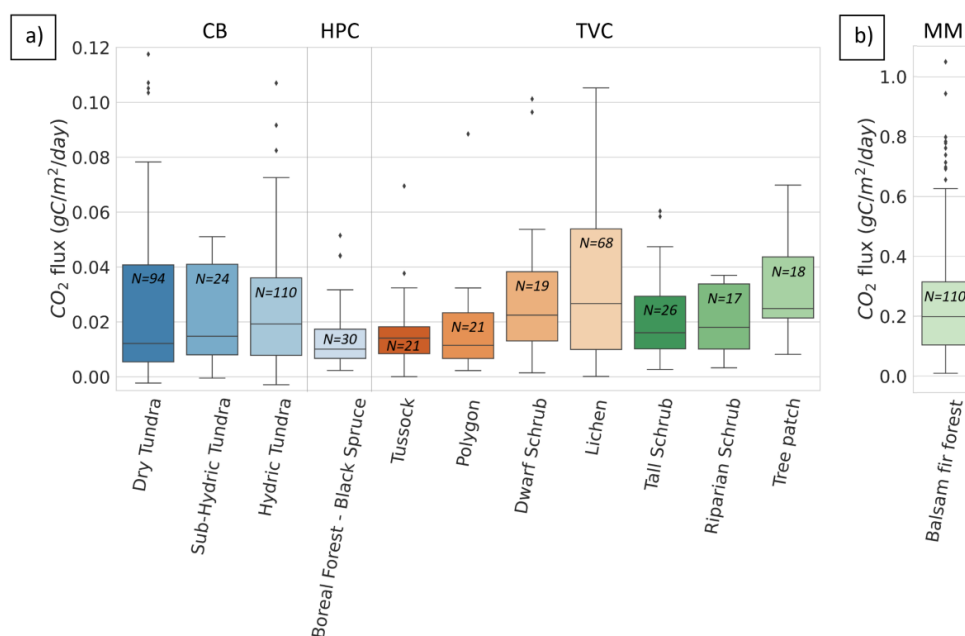
3.2.4 Vegetation types

Figure 8 shows non-growing season F_{CO_2} across the four study sites for different vegetation types. Since CB vegetation is mostly prostrate-shrub tundra, CB ecosystems were regrouped by water availability. 395 Median non-growing season F_{CO_2} at CB were observed in environments experiencing wetter conditions during the growing season. At TVC, several vegetation and land cover types are present. F_{CO_2} from MM were higher than for the other sites. Higher F_{CO_2} can be explained by warmer mean annual average temperature, a deeper snowpack and winter T_{soil} around $0^\circ C$ (See Sect. 3.4).

400 Vegetation type was not identified as a strong predictor of F_{CO_2} by the RF model. Nonetheless, we observed differences in the mean and range of F_{CO_2} for the various vegetation types probed in this study. This might be due to the strong correlation between vegetation type and soil temperature (Fig. A3), as well as relationships between vegetation and soil type, including soil organic matter content and soil pore size. The RF algorithm showed vegetation type relative importance increased to 42% when T_{soil} was removed from the 405 environmental variables, although the removal of T_{soil} decreased RF performance substantially ($R^2 = 0.40$).



Therefore, vegetation could be used as a proxy variable for T_{soil} if the latter is not available to predict F_{CO_2} , but with poorer results.



410 **Figure 8:** Boxplot of CO₂ flux (F_{CO_2}) across 12 vegetation types and 4 sites. F_{CO_2} are on a separate scale (b) because they
 are much higher than the colder environments. Cambridge Bay (CB) sites are ordered by increasing water availability
 and Trail Valley Creek (TVC) sites are ordered by increasing soil surface temperature in March 2021 and 2022. Havikpak
 415 Creek (HPC) and Montmorency Forest (MM) were composed of a single vegetation type. Outliers were defined as F_{CO_2}
 $> Q_3 + 1.5 \text{ IQR}$ where Q_3 is the third quartile and IQR the interquartile range. Outliers are out of y-axis range for the dry
 tundra (4), sub-hydric tundra (4), hydric tundra (4) and lichen (3). The outliers can be found in Fig. 5.

4 Discussion

4.1 Controls of non-growing season CO₂ fluxes

The RF model supported that T_{soil} was the dominant predictor of non-growing season F_{CO_2} when the soil
 420 was frozen. However, in the closed-boreal forest site where the zero-curtain conditions remained throughout
 the winter, LWC became the most important predictor. Our results corroborate the strong non-growing season
 F_{CO_2} dependency on T_{soil} shown by Natali et al. (2019), although we observed fluxes lower than reported by
 Natali et al. (2019) at $T_{\text{soil}} < -5^\circ\text{C}$ and mostly higher fluxes at $T_{\text{soil}} > -5^\circ\text{C}$. It should be noted that the Natali
 et al. (2019) regression was obtained using F_{CO_2} estimates from several methods including eddy covariance,
 425 chamber and snowpack diffusion measurements, whereas our study exclusively uses the latter. Several
 studies have shown bias between the different measurement methods; eddy covariance and soil chamber
 methods displayed positive biases when compared to snowpack diffusion measurements (McDowell et al.,



2000; Björkman et al., 2010a; Webb et al., 2016), while the snow chamber displayed negative biases when compared to the snowpack diffusion measurements (McDowell et al., 2000).

430 4.2 Zero-curtain conditions

Soil LWC was observed only at the MM site, where T_{soil} was around 0°C throughout winter. In zero-curtain conditions, LWC was shown to become the dominant control of non-growing season F_{CO_2} , while T_{soil} importance diminished. Our study highlighted the important impact of LWC on F_{CO_2} around soil freezing point when there is a mixed state of ice and free water in soil. When the soil is at zero-curtain, the latent heat
435 governs the ice and liquid water ratio in the soil (Devoie et al., 2022). Hence, LWC and ice fractions can be used as a freezing/thawing indicator during the zero-curtain period and help better quantify the F_{CO_2} fluxes in boreal forest environment where zero-curtain conditions prevail (Prince et al., 2019). This result is particularly important in ABR since the duration and frequency of zero-curtain periods are expected to increase in a warming climate (Yi et al., 2015 and 2019, Tao et al., 2021). It should be noted that one of the
440 measurement locations at MM displayed low F_{CO_2} despite its LWC being the highest of all sites. The soil composition of this site consisted of a thick (> 30 cm) soil organic top layer, whereas all other measurements were done at sites with thinner (3-10 cm) organic layers on top of mineral soil. It is well known that anaerobic conditions created by high soil moisture (at least $> 50\%$) constrain soil CO_2 respiration rates during the growing season because many microorganisms require oxygen for organic matter decomposition which they
445 lack if soil porosities are filled with water (Linn and Doran, 1984; Davidson and Janssens, 2006).

4.3 Snowpack importance

Our study shows that abiotic variables related to T_{soil} , LWC, and physical snowpack properties explain the majority of variance in winter CO_2 fluxes. It should be noted that we did not incorporate variables related to temporal dynamics such as the previous days' soil temperature and LWC, which have been shown by Harel
450 et al. (2023) to be of importance during the growing season. However, winter soil variables are not expected to be as dynamic as during the growing season because of the snowpack insulating properties. The RF model showed that SWE and mean snow density were the snow characteristics that provided the greatest improvement of the RF model, although to a lesser degree than T_{soil} and LWC. The importance of snow characteristics in F_{CO_2} is linked with the strong correlation to T_{soil} (Dominé et al., 2016a), although a snapshot
455 of snow conditions provides limited abilities to infer T_{soil} as shown in Slater et al. (2017). Snow properties temporal information is required to predict the impact of snow insulation on T_{soil} , with the most important period being in the autumn freeze-up when air temperature decreases below the freezing point. Snow characteristics are closely linked to topography (Meloche et al., 2021), and thus soil wetness and soil carbon content (Gouttevin et al., 2012).



460 4.4 Soil biogeochemistry

The unexplained variance (16%) suggests that winter CO₂ fluxes might have been controlled by other environmental variables such as soil physical-chemical properties regulating soil biogeochemistry and soil redox conditions, which were not addressed in this study. CO₂ production is governed by the availability of labile C compounds regulating the decomposition of soil organic matter (Michaelson et al., 2005; Wang et al., 2011), and the activity and composition of the soil microbial community (Monson et al., 2006). Soil type and structure, for example the thickness of the organic layer, soil pore size distribution, as well as soil pH may be further strong controls on CO₂ production (Steponavičienė et al., 2022; Yli-Halla et al., 2022). All these variables vary widely across the heterogeneous tundra terrain (Virtanen and Ek, 2014), where small-scale moisture, vegetation and soil conditions occur among hummock and inter-hummock depressions (Wilcox et al. 2019). Further analysis is required to understand the role of physical-chemistry soil properties on F_{CO₂} during the non-growing season.

4.5 Relevance for terrestrial biosphere models

Large uncertainties remain in terrestrial biosphere models used to estimate CO₂ fluxes in the ABR (Fisher et al., 2014; Tei and Sugimoto, 2020; Birch et al., 2021; Virkkala et al., 2021), especially regarding the respiratory release of CO₂ via soil respiration (the sum of heterotrophic respiration and belowground autotrophic respiration) during the non-growing season (Natali et al., 2019). The limited number of observational data available has restricted model improvements, testing, and evaluation (Virkkala et al., 2022). Modelling the ABR carbon cycle is critical for climate projections since a warmer climate should lead to higher T_{soil}, thus increasing ABR non-growing season F_{CO₂} (Mellander et al., 2007; Throop et al., 2012; Wieder et al., 2019). Several terrestrial biosphere models are currently in use (Fisher et al., 2022), such as CLM (Community Land Model; Lawrence et al., 2019) and CLASSIC (Canadian Land Surface Scheme Including Biogeochemical Cycles; Melton et al., 2020; Seiler et al., 2021). The F_{CO₂} relationships to T_{soil} and LWC observed in this study could be used to inform terrestrial biosphere models through the parametrization of non-growing season soil respiration sensitivity to soil temperature (e.g., Q₁₀) and LWC in zero-curtain conditions. Our study shows that permanent installation of the snow gradient method (Seok et al., 2009; Zhu et al., 2014; Graham and Risk, 2018) would be suitable to gather temporal non growing season CO₂ fluxes in ABR required to fully test terrestrial biospheres models.

5 Conclusion

Our study showed that T_{soil} is the main control of non-growing season F_{CO₂} at T_{soil} < 0°C in ABR. The relative importance analysis of our RF model showed that T_{soil} was the main predictor of F_{CO₂}, followed by LWC. However, we found that at our site maintaining zero-curtain conditions throughout winter, LWC becomes the main control of non-growing season F_{CO₂}. We observed non-negligible non-growing season F_{CO₂} that may partially offset growing season CO₂ uptake in ABR. Consequently, non-growing season F_{CO₂}



495 must be properly estimated in terrestrial biosphere models and climate models. Additionally, future research
should focus on linking the effects of abiotic variables on F_{CO_2} during the non-growing season, as we
determined here, with soil biogeochemistry, microbial functioning and vegetation.

6 Acknowledgements

This work was made possible thanks to the contributions of the Natural Sciences and Engineering Research
Council of Canada (NSERC), the Fonds de recherche du Québec – Nature et technologies (FRQNT) and
500 Polar Knowledge Canada (POLAR). A special thanks to everybody that contributed to data collection and
gas analyzing: Elise Imbeau (Viventem), Gabriel Ferland (Viventem), Aili Pedersen (POLAR), Gabriel
Hould Gosselin (Université de Montréal [UdeM] and Wilfrid Laurier University [WLU]), Emma Riley
(WLU), Rosy Tutton (WLU), Victoria Dutch (Northumbria University [NU]), Georgina Woolley (NU), Élise
Groulx (Université de Sherbrooke [UdeS]), Charlotte Crevier (UdeS), Érika Boisvert (UdeS), Alain Royer
505 (UdeS), Patrick Ménard (UdeS), Vincent Sasseville (UdeS), Célia Trunz (UdeS), Daniel Kramer (UdeS),
Estéban Hamel Jomphe (UQTR), Samuel Goulet (UQTR), Alex Gélinas (UQTR), David de Courville
(UQTR), Juliette Ortet (UQTR) and Chris Derksen (Environment and Climate Change Canada). We would
also like to thank Ian Hogg, Johann Wagner and Scott Johnson from POLAR for their logistical support.

7 Competing interests

510 The authors declare that they have no conflict of interest.

8 Data availability

Mavrovic, A., Sonnentag, O., Voigt, C., Roy, A. (2023). Non-growing season CO₂ fluxes over arctic and
boreal environments. *Borealis*, V1, UNF:6:u35JsrWpGNJSM3chSR9Ssg== [fileUNF]. doi:
515 10.5683/SP3/R3KZEQ

520

525



References

- 530 Baldocchi, D., Falge, E., Gu, L., Olson, R., Hollinger, D., Running, S., Anthoni, P., Bernhofer, C., Davis, K., Evans, R.,
Fuentes, J., Goldstein, A., Katul, G., Law, B., Lee, X., Malhi, Y., Meyers, T., Munger, W., Oechel, W., Paw
U, K., Pilegaard, K., Schmid, H., Valentini, R., Verma, S., Vesala, T., Wilson, K., and Wofsy, S.: FLUXNET:
A New Tool to Study the Temporal and Spatial Variability of Ecosystem–Scale Carbon Dioxide, Water Vapor,
and Energy Flux Densities. *Bull. Am. Meteorol.*, 82(11), 2415–2434, doi: 10.1175/1520-
0477(2001)082<2415:fantts>2.3.co;2, 2001.
- 535 Baldocchi, D.: Assessing the eddy covariance technique for evaluating carbon dioxide exchange rates of ecosystems :
past, present and future. *Glob. Chang. Biol.*, 9(4), 479–492, doi: 10.1046/j.1365-2486.2003.00629.x, 2003.
- 540 Barry R, Plamondon, AP, and Stein, J.: Hydrologic soil properties and application of a soil moisture model in a balsam
fir forest. *Can. J. For. Res.*, 18(4), 427–434, doi: 10.1139/x88-063, 1988.
- 545 Biasi, C., and van Delden, L.: Field protocol : Determination of soil N₂O fluxes by a diffusion gradient method - Version
1. NOCA Project, Department of Environmental and Biological Sciences, University of Eastern Finland,
Kuopio, Finland, 14 pages, 2019.
- Birch, L., Schwalm, C., Natali, S., Lombardozi, D., Keppel-Aleks, G., Watts, J., Lin, X., Zona, D., Oechel, W., Sachs,
T., Black, T. A., and Rogers, B.: Addressing biases in Arctic–boreal carbon cycling in the Community Land
Model Version 5. *Geosci. Model Dev. Discuss.*, 14, 3361–3382, doi: 10.5194/gmd-14-3361-2021, 2021.
- 550 Björkman, M., Morgner, E., Cooper, E., Elberling, B., Klemetsson, L., and Björk, R.: Winter carbon dioxide effluxes
from Arctic ecosystems : An overview and comparison of methodologies. *Glob. Biogeochem. Cycles*, 24,
GB3010, doi: 10.1029/2009GB003667, 2010.
- 555 Bond-Lamberty, B., and Thomson, A.: Temperature-associated increases in the global soil respiration record. *Nature*,
464, 579–582, doi:10.1038/nature08930, 2010.
- Bouyoucos, G.J.: Hydrometer Method Improved for Making Particle Size Analyses of Soils. *Agron. J.*, 54(5), 464–465,
doi: 10.2134/agronj1962.00021962005400050028x, 1962.
- 560 Bowley, A.: The Standard Deviation of the Correlation Coefficient. *J. Am. Stat. Assoc.*, 23(161), 31–34,
doi:10.2307/2277400, 1928.
- 565 Braghieri, R., Fisher, J., Miner, K., Miller, C., Worden, J., Schimel, D., and Frankenberg, C.: Tipping point in North
American Arctic–Boreal carbon sink persists in new generation Earth system models despite reduced
uncertainty. *Environ. Res. Lett.*, 18(2), 025008, doi: 10.1088/1748-9326/acb226, 2023
- Breiman, L.: Random forests. *Mach. Learn.*, 45, 5–32, doi: 10.1023/A:1010933404324, 2001.



- 570 Brown, J., Ferrians, O., Heginbottom, J., and Melnikov, E.: Circum-Arctic Map of Permafrost and Ground-Ice Conditions, Version 2. Boulder, Colorado USA. NSIDC: National Snow and Ice Data Center, doi: 10.7265/skbg-kf16, 2002.
- 575 Bruhwiler, L., Parmentier, F.-J., Crill, P., Leonard, M., and Palmer, P.: The Arctic Carbon Cycle and Its Response to Changing Climate. *Curr. Clim. Change Rep.*, 7, 14-34, doi: 10.1007/s40641-020-00169-5, 2021.
- Busseau, B.-C., Royer, A., Roy, A., Langlois, A., and Dominé, F.: Analysis of snow-vegetation interactions in the low Arctic-Subarctic transition zone (northeastern Canada). *Phys. Geogr.*, 38(2), 159-175, doi: 0.1080/02723646.2017.1283477, 2017.
- 580 Callaghan, T., Johansson, M., Brown, R., Groisman, P., Labba, N., Radionov, V., Bradley, R., Blangy, S., Bulygina, O., Christensen, T., Colman, J., Essery, R., Forbes, B., Forchhammer, M., Golubev, V., Honrath, R., Juday, G., Meshcherskaya, A., Phoenix, G., Pomeroy, J., Rautio, A., Robinson, D., Schmidt, N., Serreze, M., Shevchenko, V., Shiklomanov, A., Shmakin, A., Sköld, P., Sturm, M., Woo, M.-k., and Wood, E.: Multiple Effects of Changes in Arctic Snow Cover. *Ambio*, 40, 32-45, doi: 10.1007/s13280-011-0213-x, 2011a.
- 585 Callaghan, T., Tweedie, C., Akerman, J., Andrews, C., Bergstedt, J., Butler, M., Christensen, T., Cooley, D., Dahlberg, U., Danby, R., Daniëls, F., de Molenaar, J., Dick, J., Mortensen, C. E., Ebert-May, D., Emanuelsson, U., Eriksson, H., Hedenäs, H., Henry, G., Hik, D., Hobbie, J., Jantze, E., Jaspers, C., Johansson, C., Johansson, M., Johnson, D., Johnstone, J., Jonasson, C., Kennedy, C., Kenney, A., Keuper, F., Koh, S., Krebs, C., Lantuit, H., Lara, M., Lin, D., Lougheed, V., Madsen, J., Matveyeva, N., McEwen, D., Myers-Smith, I., Narozhniy, Y., Olsson, H., Pohjola, V., Price, L., Rigét, F., Rundqvist, S., Sandström, A., Tamstorf, M., Bogaert, R. V., Villareal, S., Webber, P., and Zemtsov, V.: Multi-Decadal Changes in Tundra Environments and Ecosystems: Synthesis of the International Polar Year-Back to the Future Project (IPY-BTF). *Ambio*, 40(6), 705-716, doi: 10.1007/s13280-011-0179-8, 2011b.
- 595 Canadian Forest Inventory Committee: Canada's National Forest Inventory ground sampling guidelines: specifications for ongoing measurement. Pacific Forestry Centre, Victoria, British Columbia, Canada, Catalog ID 29402, ISBN 978-1-100-11329-6, 271 pages, 2008.
- 600 Carreiras, J., Quegan, S., Le Toan, T., Ho Tong Minh, D., Saatchi, S., Carvalhais, N., Reichstein, M., and Scipal, K.: Coverage of high biomass forests by the ESA BIOMASS mission under defense restrictions. *Remote Sens. Environ.*, 196, 154-162, doi: 10.1016/j.rse.2017.05.003, 2017.
- 605 Christiansen, C., Schmidt, N., and Michelsen, A.: High Arctic dry heath CO₂ exchange during the early cold season. *Ecosystems*, 15(7), 1083–1092, doi: 10.1007/s10021-012-9569-4, 2012.
- Davidson, E., and Janssens, I.: Temperature sensitivity of soil carbon decomposition and feedbacks to climate change. *Nature*, 440, 165–173, doi:10.1038/nature04514, 2006.



- 610 Derksen, C., Burgess, D., Duguay, C., Howell, S., Mudryk, L., Smith, S., Thackeray, C., and Kirchmeier-Young, M.: Changes in snow, ice, and permafrost across Canada. Canada's Changing Climate Report – Chapter 5, Government of Canada, Ottawa, Ontario, Canada, 194–260, 2019.
- Devoie, É., Gruber, S., and McKenzie, J.: A repository of measured soil freezing characteristic curves: 1921 to 2021. 615 Earth Syst. Sci. Data, 14(7), 3365–3377, doi: 10.5194/essd-14-3365-2022, 2022.
- Dominé, F., Barrère, M., Sarrazin, D., Morin, S., and Arnaud, L.: Automatic monitoring of the effective thermal conductivity of snow in a low-Arctic shrub tundra. Cryosphere, 9(3), 1265–1276, doi: 10.5194/tc-9-1265-2015, 2015. 620
- Dominé, F., Barrère, M., and Sarrazin, D.: Seasonal evolution of the effective thermal conductivity of the snow and the soil in high Arctic herb tundra at Bylot Island, Canada. Cryosphere, 10, 2573–2588, doi: 10.5194/tc-10-2573-2016, 2016a.
- 625 Dominé, F., Barrère, M., and Morin, S.: The growth of shrubs on high Arctic tundra at Bylot Island: Impact on snow physical properties and permafrost thermal regime. Biogeosciences, 13(23), 6471–6486, doi: 10.5194/bg-13-6471-2016, 2016b.
- Dominé, F., Fourteau, K., Picard, G., Lackner, G., Sarrazin, D., and Poirier, M.: Permafrost cooled in winter by thermal bridging through snow-covered shrub branches. Nat. Geosci., 15, 554–560, doi: 10.1038/s41561-022-00979-2, 2022. 630
- Elberling, B.: Annual soil CO₂ effluxes in the High Arctic: The role of snow thickness and vegetation type. Soil Biol. Biochem., 39(2), 646–654, doi: 10.1016/j.soilbio.2006.09.017, 2007. 635
- Fooladmand, H. R.: Estimating soil specific surface area using the summation of the number of spherical particles and geometric mean particle-size diameter. Afr. J. Agric. Res., 6(7), 1758–1762, doi: 10.5897/AJAR11.19, 2011.
- 640 Fisher, J., Sikka, M., Oechel, W., Huntzinger, D., Melton, J., Koven, C., Ahlström, A., Arain, M., Baker, I., Chen, J., Ciais, P., Davidson, C., Dietze, M., El-Masri, B., Hayes, D., Huntingford, C., Jain, A., Levy, P., Lomas, R., Poulter, B., Price, D., Sahoo, A., Schaefer, K., Tian, H., Tomelleri, E., Verbeeck, H., Viovy, N., Wania, R., Zeng, N., and Miller, C.: Carbon cycle uncertainty in the Alaskan Arctic. Biogeosciences, 11(15), 4271–4288, doi: 10.5194/bg-11-4271-2014, 2014.
- 645 Fisher, J., Sikka, M., Block, G., Schwalm, C., Parazoo, N., Kolus, H., Sok, M., Wang, A., Gagne-Landmann, A., Lawal, S., Guillaume, A., Poletti, A., Schaefer, K., El Masri, B., Levy, P., Wei, Y., Dietze, M., and Huntzinger, D.: The Terrestrial Biosphere Model Farm. J. Adv. Model Earth Syst., 14(2), e2021MS002676, doi: 10.1029/2021MS002676, 2022.
- 650 Gauthier, S., Bernier, P., Kuuluvainen, T., Shvidenko, A., and Schepaschenko, D.: Boreal forest health and global change. Science, 349(6250), 819–822, doi: 10.1126/science.aaa9092, 2015.



- 655 Gouttevin, I., Menegoz, M., Dominé, F., Krinner, G., Koven, C., Ciais, P., Tarnocai, C., and Boike, J.: How the insulating properties of snow affect soil carbon distribution in the continental pan-Arctic area. *Biogeosciences*, 117(G2), G02020, doi: 10.1029/2011JG001916, 2012.
- Graham, L., and Risk, D.: Explaining CO₂ fluctuations observed in snowpacks. *Biogeosciences*, 15(3), 847–859, doi:10.5194/bg-15-847-2018, 2018.
- 660 Grünberg, I., Wilcox, E., Zwieback, S., Marsh, P., and Boike, J.: Linking tundra vegetation, snow, soil temperature, and permafrost. *Biogeosciences*, 17(16), 4261–4279, doi: 10.5194/bg-17-4261-2020, 2020.
- Harel, A., Sylvain, J., Drolet, G., Thiffault, E., Thiffault, N., and Tremblay, S.: Fine scale assessment of seasonal, intra-seasonal and spatial dynamics of soil CO₂ effluxes over a balsam fir-dominated perhumid boreal landscape. *Agric. For. Meteorol.*, 335, 109469, doi: 10.1016/j.agrformet.2023.109469, 2023.
- 665 Harvey, A., In Haynes, W., Lide, D., and Bruno, T.: *CRC Handbook of Chemistry and Physics (97th ed.): Properties of Ice and Supercooled Water*. CRC Press, Boca Raton, Florida, United States, 2666 pages (6-12). ISBN 978-1-4987-5429-3, 2017.
- 670 Hayes, J., McGuire, A., Kicklighter, D., Gurney, K., Burnside, T., and Melillo, J.: Is the northern high-latitude land-based CO₂ sink weakening?. *Glob. Biogeochem. Cycles*, 25(3), GB3018, doi: 10.1029/2010GB003813, 2011.
- van Huissteden, J., and Dolman, A.: Soil carbon in the Arctic and the permafrost carbon feedback. *Current Opinion in Environmental Sustainability*, 4(5), 545–551, doi: 10.1016/j.cosust.2012.09.008, 2012.
- 675 Jentzsch, K., Boike, J., and Foken, T.: Importance of the Webb, Pearman, and Leuning (WPL) correction for the measurement of small CO₂ fluxes. *Atmos. Meas. Tech.*, 14(11), 7291–7296, doi: 10.5194/amt-14-7291-2021, 2021.
- 680 Jones, H., Pomeroy, J., Davies, T., Tranter, M., and Marsh, P.: CO₂ in Arctic snow cover: landscape form, in-pack gas concentration gradients, and the implications for the estimation of gaseous fluxes. *Hydrol. Process.*, 13–18, 2977–2989, doi: 10.1002/(SICI)1099-1085(19991230)13:18<2977::AID-HYP12>3.0.CO;2-%23, 1999.
- 685 Kibitía, H., Abdullah, S., and Bustamam, A.: Comparison of random forest and support vector machine for prediction of cognitive impairment in Parkinson's disease. *AIP Conf. Proc.*, 2296(1), 020093, doi: 10.1063/5.0030332, 2020.
- Kim, Y., Tsunogai, S., and Tanaka, N.: Winter CO₂ emission and its production rate in cold temperate soils of northern Japan: ²²²Rn as a proxy for the validation of CO₂ diffusivity. *Polar Sci.*, 22, 100480, doi: 10.1016/j.polar.2019.09.002, 2019.
- 690 Kinar, N., and Pomeroy, J.: Measurement of the physical properties of the snowpack. *Rev. Geophys.*, 53(2), 481–544, doi: 10.1002/2015RG00048, 2015.



- 695 Knowles, J., Blanken, P., and Williams, M.: Soil respiration variability across a soil moisture and vegetation community gradient within a snow-scoured alpine meadow. *Biogeochemistry* 125, 185–202, doi: 10.1007/s10533-015-0122-3, 2015.
- 700 Koven, C., Riley, W., Subin, Z., Tang, J., Torn, M., Collins, W., Bonan, G., Lawrence, D., and Swenson, S.: The effect of vertically resolved soil biogeochemistry and alternate soil C and N models on C dynamics of CLM4. *Biogeosciences*, 10(11), 7109-7131, doi: 10.5194/bg-10-7109-2013, 2013.
- 705 Krogh, S., Pomeroy, J., and Marsh, P.: Diagnosis of the hydrology of a small Arctic basin at the tundra-taiga transition using a physically based hydrological model. *J. Hydrol.*, 550, 685-703, doi: 10.1016/j.jhydrol.2017.05.042, 2017.
- 710 Kropp, H., Loranty, M., Rutter, N., Fletcher, C., Derksen, C., Mudryk, L., and Todt, M.: Are vegetation influences on Arctic–boreal snow melt rates detectable across the Northern Hemisphere?. *Environ. Res. Lett.*, 17, 104010, doi: 10.1088/1748-9326/ac8fa7, 2022.
- 715 Lawrence, D., Fisher, R., Koven, C., Oleson, K., Swenson, S., Bonan, G., Collier, N., Ghimire, B., Kampenhout, L., Kennedy, D., Kluzek, E., Lawrence, P., Li, F., Li, H., Lombardozzi, D., Riley, W., Sacks, W., Shi, M., Vertenstein, M., Wieder, W., Xu, C., Ali, A., Badger, A., Bisht, G., Broeke, M., Brunke, M., Burns, S., Buzan, J., Clark, M., Craig, A., Dahlin, K., Drewniak, B., Fisher, J., Flanner, M., Fox, A., Gentine, P., Hoffman, F., Keppel-Aleks, G., Knox, R., Kumar, S., Lenaerts, J., Leung, L. R., Lipscomb, W., Lu, Y., Pandey, A., Pelletier, J., Perket, J., Randerson, J., Ricciuto, D., Sanderson, B., Slater, A., Subin, Z., Tang, J., Thomas, R. Q., Val Martin, M., and Zeng, X.: The Community Land Model version 5: Description of new features, benchmarking, and impact of forcing uncertainty. *J. Adv. Model. Earth Syst.*, 11(12), 4245–4287, doi:10.1029/2018MS001583, 2019.
- 720 Leclerc, M., and Thurtell, G.: Footprint prediction of scalar fluxes using a Markovian analysis. *Bound.-Layer Meteorol.*, 52(3), 247-258, doi: 10.1007/BF00122089, 1990.
- 725 Liaw, A., and Wiener, M.: Classification and Regression by Randomforest. *R News*, 2(3), 18-22, 2002.
- Linn, D., and Doran, J.: Effect of Water Filled Pore Space on Carbon Dioxide and Nitrous Oxide Production in Tilled and Non-Tilled Soils. *Soil Sci. Soc. Am. J.*, 48(6), 1267-1272, doi: 10.2136/sssaj1984.03615995004800060013x, 1984.
- 730 Loranty, M., Abbott, B., Blok, D., Douglas, T., Epstein, H., Forbes, B., Jones, B., Kholodov, A., Kropp, H., Malhotra, A., Mamet, S., Myers-Smith, I., Natali, S., O'Donnell, J., Phoenix, G., Rocha, A., Sonnentag, O., Tape, K., and Walker, D.: Reviews and syntheses: Changing ecosystem influences on soil thermal regimes in northern high-latitude permafrost regions. *Biogeosciences*, 15(17), 5287–5313, doi:10.5194/bg-15-5287-2018, 2018.



- 735 Maier, M., Weber, T., Fiedler, J., Fuß, R., Glatzel, S., Huth, V., Jordan, S., Jurasinski, G., Kutzbach, L., Schäfer, K., Weymann, D., and Hagemann, U.: Introduction of a guideline for measurements of greenhouse gas fluxes from soils using non-steady-state chambers. *J. Soil Sci. Plant Nutr.*, 185(4), 447-461, doi: 10.1002/jpln.202200199, 2022.
- 740 Marrero, T., and Mason E.: Gaseous diffusion coefficients. *J. Phys. Chem. Ref. Data*, 1(1), 3-117, doi: 10.1063/1.3253094, 1972.
- Martin, M., Kumar, P., Sonnentag, O., and Marsh, P.: Thermodynamic basis for the demarcation of Arctic and alpine treelines. *Sci. Rep.*, 12, 12565, doi: 10.1038/s41598-022-16462-2, 2022.
- 745 Massman, W.: A review of the molecular diffusivities of H₂O, CO₂, CH₄, CO, O₃, SO₂, NH₃, N₂O, NO, and NO₂ in air, O₂ and N₂ near STP. *Atmos. Environ.*, 32(6), 1111-1127, doi: 10.1016/S1352-2310(97)00391-9, 1998.
- 750 Mast, M. A., Wickland, K., Striegl, R., and Clow, D.: Winter fluxes of CO₂ and CH₄ from subalpine soils in Rocky Mountain National Park, Colorado. *Glob. Biogeochem. Cycles*, 12(4), 607-620, doi: 10.1029/98GB02313, 1998.
- McDowell, N., Marshall, J., Hooker, T., and Musselman, R.: Estimating CO₂ flux from snowpacks at three sites in the Rocky Mountains. *Tree physiol.*, 20(11), 745-753, doi: 10.1093/treephys/20.11.745, 2000.
- 755 McGuire, D., Anderson, L., Christensen, T., Dallimore, S., Guo, L., Hayes, D., Heimann, M., Lorensen, T., MacDonald, R., and Roulet, N.: Sensitivity of the carbon cycle in the Arctic to climate change. *Ecological Monographs*, 79(4), 523-555, doi: 10.1890/08-2025.1, 2009.
- 760 McMahon, S., Parker, G., and Miller, D.: Evidence for a recent increase in forest growth. *Proc. Natl. Acad. Sci. U.S.A.*, 107(8), 3611-3615, doi: 10.1073/pnas.0912376107, 2010.
- Mellander, P., Löfvenius, M., and Laudon, H.: Climate change impact on snow and soil temperature in boreal Scots pine stands. *Clim. Change*, 85, 179-193, doi:10.1007/s10584-007-9254-3, 2007.
- 765 Meloche, J., Langlois, A., Rutter, N., McLennan, D., Royer, A., Billecocq, P., and Ponomarenko, S.: High-resolution snow depth prediction using Random Forest algorithm with topographic parameters: A case study in the Greiner watershed, Nunavut. *Hydrol. Process.*, 36(3), e14546, doi: 10.1002/hyp.14546, 2021.
- 770 Melton, J., Arora, V., Wisernig-Cojoc, E., Seiler, C., Fortier, M., Chan, E., and Teckentrup, L.: CLASSIC v1.0: the open-source community successor to the Canadian Land Surface Scheme (CLASS) and the Canadian Terrestrial Ecosystem Model (CTEM) – Part 1: Model framework and site-level performance. *Geosci. Model Dev.*, 13(6), 2825-2850, doi: 10.5194/gmd-13-2825-2020, 2020.
- 775 Ménard, C., Essery, R., Pomeroy, J., Marsh, P., and Clark, D.: A shrub bending model to calculate the albedo of shrub-tundra. *Hydrol. Process.*, 28(2), 341-351, doi: 10.1002/hyp.9582, 2012.



- 780 Michaelson, G. J., and Ping, C. L.: Soil organic carbon and CO₂ respiration at subzero temperature in soils of Arctic Alaska. *J. Geophys. Res. Atmos.* 108(D2), 8164, doi: 10.1029/2001JD000920, 2005.
- Millington, R. J.: Gas Diffusion in Porous Media. *Science*, 130(3367), 100-102, doi: 10.1126/science.130.3367.100-a, 1959.
- 785 Miner, K., Turetsky, M., Malina, E., Bartsch, A., Tamminen, J., McGuire, A. D., Fix, A., Sweeney, C., Elder, C., and Miller, C.: Permafrost carbon emissions in a changing Arctic. *Nat. Rev. Earth Environ.*, 3, 55–67, doi:10.1038/s43017-021-00230-3, 2022.
- 790 Monson, R., Lipson, D., Burns, S., Turnipseed, A., Delany, A., Williams, M., and Schmidt, S.: Winter forest soil respiration controlled by climate and microbial community composition. *Nature*, 439, 711–714, doi: 10.1038/nature04555, 2006.
- 795 Myers-Smith, I. H., Kerby, J., Phoenix, G., Bjerke, J., Epstein, H., Assmann, J., John, C., Andreu-Hayles, L., Angers-Blondin, S., Beck, P., Berner, L., Bhatt, U., Björkman, A., Blok, C., Bryn, A., Christiansen, C., Cornelissen, J. H. C., Cunliffe, A., Elmendorf, S., Forbes, B., Goetz, S., Hollister, R., de Jong, R., Loranty, M., Macias-Fauria, M., Maseyk, K., Normand, S., Olofsson, J., Parker, T., Parmentier, F.-J., Post, E., Schaeppman-Strub, G., Stordal, F., Sullivan, P., Thomas, H., Tømmervik, H., Treharne, R., Tweedie, C., Walker, D., Wilmking, M., and Wipf, S.: Complexity revealed in the greening of the Arctic. *Nat. Clim. Change*, 10, 106-117, doi: 10.1038/s41558-019-0688-1, 2020.
- 800 Natali, S., Watts, J., Rogers, B., Potter, S., Ludwig, S., Selbmann, A.-K., Sullivan, P., Abbott, B., Arndt, K., Birch, L., Björkman, M., Bloom, A., Celis, G., Christensen, T., Christiansen, C., Commane, R., Cooper, E., Crill, P., Czimczik, C., Davydov, S., Du, J., Egan, J., Elberling, B., Euskirchen, E., Friborg, T., Genet, H., Göckede, M., Goodrich, J., Grogan, P., Helbig, M., Jafarov, E., Jastrow, J., Kalhori, A., Kim, Y., Kimball, J., Kutzbach, L., Lara, M., Larsen, K., Lee, B.-Y., Liu, Z., Loranty, M., Lund, M., Lupascu, M., Madani, N., Malhotra, A., 805 Matamala, R., McFarland, J., McGuire, A., Michelsen, A., Minions, C., Oechel, W., Olefeldt, D., Parmentier, F.-J., Pirk, N., Poulter, B., Quinton, W., Rezanezhad, F., Risk, D., Sachs, T., Schaefer, K., Schmidt, N., Schuur, E., Semenchuk, P., Shaver, G., Sonnentag, O., Starr, G., Treat, C., Waldrop, M., Wang, Y., Welker, J., Wille, C., Xu, X., Zhang, Z., Zhuang, Q., and Zona, D.: Large loss of CO₂ in winter observed across the northern permafrost region. *Nat. Clim. Change*, 9, 852-857, doi: 10.1038/s41558-019-0592-8, 2019.
- 810 Natali, S., Holdren, J., Rogers, B., Treharne, R., Duffy, P., Pomerance, R., and MacDonald, E.: Permafrost carbon feedbacks threaten global climate goals. *Proc. Natl. Acad. Sci. U.S.A.*, 118(21), e2100163118, doi: 10.1073/pnas.2100163118, 2021.
- 815 Outcalt, S., Nelson, F., and Hinkel, K.: The zero-curtain effect: Heat and mass transfer across an isothermal region in freezing soil. *Water Resour. Res.*, 26(7), 1509-1516, doi: 10.1029/WR026i007p01509, 1990.



- 820 Pallandt, M., Kumar, J., Mauritz, M., Schuur, E., Virkkala, A.-M., Celis, G., Hoffman, F., and Göckede, M.: Representativeness assessment of the pan-Arctic eddy-covariance site network, and optimized future enhancements. *Biogeosciences*, 19(3), 559-583, doi: 10.5194/bg-19-559-2022, 2022.
- Pastorello, G., Trotta, C., Canfora, E., et al.: The FLUXNET2015 dataset and the ONEFlux processing pipeline for eddy covariance data. *Sci. Data*, 7, 225, doi: 10.1038/s41597-020-0534-3, 2020.
- 825 Pirk, N., Tamstorf, M., Lund, M., Mastepanov, M., Pedersen, S., Myllus, M., Parmentier, F.-J., Christiansen, H., and Christensen: Snowpack fluxes of methane and carbon dioxide from high Arctic tundra. *Biogeosciences*, 12(11), 2886-2900, doi: 10.1002/2016JG003486, 2016.
- Ponomarenko, S., McLennan, D., Pouliot, D., and Wagner, J.: High Resolution Mapping of Tundra Ecosystems on 830 Victoria Island, Nunavut – Application of a Standardized Terrestrial Ecosystem Classification. *Can. J. Remote.*, 45(5), 551-571, doi: 10.1080/07038992.2019.1682980, 2019.
- Potapov, P., Hansen, M., Stehman, S., Loveland, T., and Pittman, K.: Combining MODIS and Landsat imagery to estimate and map boreal forest cover loss. *Remote Sens Environ.*, 112(9), 3708-3719, doi: 835 10.1016/j.rse.2008.05.006, 2008.
- Prieur du Plessis, J., and Masliyah, J.: Flow through isotropic granular porous media. *Transp. Porous Media*, 6(3), 207–221, doi: 10.1007/BF00208950, 1991.
- 840 Prince, M., Roy, A., Brucker, L., Royer, A., Kim, Y., and Zhao, T.: Northern Hemisphere surface freeze–thaw product from Aquarius L-band radiometers. *Eath Syst. Sci. Data*, 10(4), 2055-2067, doi: 10.5194/essd-10-2055-2018, 2018.
- 845 Prince, M., Roy, A., Royer, A., and Langlois, A.: Timing and spatial variability of fall soil freezing in boreal forest and its effect on SMAP L-band radiometer measurements. *Remote Sens Environ.*, 231(9), 111230, doi: 10.1016/j.rse.2019.111230, 2019.
- Proksch, M., Rutter, N., Fierz, C., and Schneebeli, M.: Intercomparison of snow density measurements: bias, precision, and vertical resolution. *Cryosphere*, 10(1), 371-384, doi: 10.5194/tc-10-371-2016, 2016.
- 850 Rantanen, M., Karpechko, A.Y., Lipponen, A., Nordling, K., Hyvärinen, O., Ruosteenoja, K., Vihma, T. and Laaksonen, A.: The Arctic has warmed nearly four times faster than the globe since 1979. *Commun. Earth Environ.*, 3(1), 1-10, doi: 10.1038/s43247-022-00498-3, 2022.
- 855 Royer, A., Dominé, F., Roy, A., Langlois, A., Marchand, N., and Davesne, G.: New northern snowpack classification linked to vegetation cover on a latitudinal mega-transect across northeastern Canada. *Écoscience*, 28(3-4), 225-242, doi: 10.1080/11956860.2021.1898775, 2021.



- 860 Schuepp, P., Leclerc, M., MacPherson, J., and Desjardins, R.: Footprint prediction of scalar fluxes from analytical solutions of the diffusion equation. *Bound.-Layer Meteorol.*, 50(1-4), 355-373, doi: 10.1007/BF00120530, 1990.
- 865 Schuur, E., McGuire, A., Schädel, C., Grosse, G., Harden, J., Hayes, D., Hugelius, G., Koven, C., Kuhry, P., Lawrence, D., Natali, S., Olefeldt, D., Romanovsky, V., Schaefer, K., Turetsky, M., Treat, C., and Vonk, J.: Climate change and the permafrost carbon feedback. *Nature*, 520, 171-179, doi: 10.1038/nature14338, 2015.
- 870 Seiler, C., Melton, J., Arora, V., and Wang, L.: CLASSIC v1.0: the open-source community successor to the Canadian Land Surface Scheme (CLASS) and the Canadian Terrestrial Ecosystem Model (CTEM) – Part 2: Global benchmarking. *Geosci. Model Dev.*, 14(5), 2371-2417, doi: 10.5194/gmd-14-2371-2021, 2021.
- Seok, B., Helmig, D., Williams, M., Liptzin, D., Chowanski, K., and Hueber, J.: An automated system for continuous measurements of trace gas fluxes through snow: an evaluation of the gas diffusion method at a subalpine forest site, Niwot Ridge, Colorado. *Biogeochemistry*, 95, 95-113, doi: 10.1007/s10533-009-9302-3, 2009.
- 875 Slater, A., Lawrence, D., and Koven, C.: Process-level model evaluation: a snow and heat transfer metric. *Cryosphere*, 11(2), 989–996, doi: 10.5194/tc-11-989-2017, 2017.
- 880 Sommerfeld, R., Mosier, A., and Musselman, R.: CO₂, CH₄ and N₂O flux through a Wyoming snowpack and implications for global budgets. *Nature*, 361, 140-142, doi: 10.1038/361140a0, 1993.
- Sommerfeld, R., Massman, W., Musselman, R., and Mosier, A.: Diffusional flux of CO₂ through snow : spatial and temporal variability among alpine–subalpine sites. *Global Biogeochem. Cycles*, 10(3), 473–482, doi: 10.1029/96GB01610, 1996.
- 885 Steponavičienė, V., Bogužas, V., Sinkevičienė, A., Skinulienė, L., Vaisvalavičius, R., and Sinkevičius, A.: Soil Water Capacity, Pore Size Distribution, and CO₂ Emission in Different Soil Tillage Systems and Straw Retention. *Plants*, 11(5), 614, doi: 10.3390/plants11050614, 2022.
- 890 Strobl, C., Boulesteix, A.-L., Kneib, T., Augustin, T., and Zeileis, A.: Conditional variable importance for random forests. *BMC Bioinform.*, 9(1), 307, doi: 10.1186/1471-2105-9-307, 2008.
- 895 Sturm, M., Schimel, J., Michaelson, G., Welker, J., Oberbauer, S., Liston, G., Fahnestock, J., and Romanovsky, V.: Winter biological processes could help convert arctic tundra to shrubland. *Bioscience*, 55, 17–26, doi: 10.1641/0006-3568(2005)055[0017:WBPCHC]2.0.CO;2, 2005.
- Subke, J., Kutzbach, L., and Risk, D.: Soil Chamber Measurements. In: *Springer Handbook of Atmospheric Measurements*. Springer Nature Switzerland AG, Cham, Switzerland, 1806 pages, doi: 10.1007/978-3-030-52171-4_60, 2021.



- 900 Tao, J., Zhu, Q., Riley, W., and Neumann, R.: Improved ELMv1-ECA Simulations of Zero-Curtain Periods and Cold-season CH₄ and CO₂ Emissions at Alaskan Arctic Tundra Sites. *Cryosphere*, 15(12), 5281-5307, doi: 10.5194/tc-2020-262, 2020.
- Tarnocai, C., Canadell, J., Schuur, E., Kuhry, P., Mazhitova, G., and Zimov, S.: Soil organic carbon pools in the northern circumpolar permafrost region. *Global Biogeochem. Cycles*, 23(2), GB2023, doi: 10.1029/2008GB003327, 2009.
- 905 Tei, S., and Sugimoto, A.: Excessive positive response of model-simulated land net primary production to climate changes over circumboreal forests. *Plant-Environment Interactions*, 1(2), 102-121, doi: 10.1002/pei3.10025, 2020.
- 910 Throop, J., Lewkowicz, A., and Smith, S.: Climate and ground temperature relations at sites across the continuous and discontinuous permafrost zones, northern Canada. *Can. J. Earth Sci.*, 49(8), 865-876, doi: 10.1139/e11-075, 2012.
- 915 Tice, A., Anderson, D., and Sterrett, K.: Unfrozen water contents of submarine permafrost determined by nuclear magnetic resonance. *Eng. Geol.*, 18(1-4), 135-146, doi:10.1016/0013-7952(81)90053-3, 1981.
- Ravn, N., Elberling, B., and Michelsen, A.: Arctic soil carbon turnover controlled by experimental snow addition, summer warming and shrub removal. *Soil Biol. Biochem.*, 142, 107698, doi: 10.1016/j.soilbio.2019.107698, 2020.
- 920 Virkkala, A.-M., Aalto, J., Rogers, B., Tagesson, T., Treat, C., Natali, S., Watts, J., Potter, S., Lehtonen, A., Mauritz, M., Schuur, E., Kochendorfer, J., Zona, D., Oechel, W., Kobayashi, H., Humphreys, E., Goeckede, M., Iwata, H., Lafleur, P., Euskirchen, E., Bokhorst, S., Marushchak, M., Martikainen, P., Elberling, B., Voigt, C., Biasi, C., Sonnentag, O., Parmentier, F.-J., Ueyama, M., Celis, G., St.Louis, V., Emmerton, C., Peichl, M., Chi, J., Järveoja, J., Nilsson, M., Oberbauer, S., Torn, M., Park, S.-J., Dolman, H., Mammarella, I., Chae, N., Poyatos, R., López-Blanco, E., Christensen, T., Kwon, M., Sachs, T., Holl, D., and Luoto, M.: Statistical upscaling of ecosystem CO₂ fluxes across the terrestrial tundra and boreal domain: Regional patterns and uncertainties. *Glob. Chang. Biol.*, 27(17), 4040-4059, doi: 10.1111/gcb.15659, 2021.
- 925 Virkkala, A.-M., Natali, S., Rogers, B., Watts, J., Savage, K., Connon, S., Mauritz, M., Schuur, E., Peter, D., Minions, C., Nojeim, J., Commane, R., Emmerton, C., Goeckede, M., Helbig, M., Holl, D., Iwata, H., Kobayashi, H., Kolari, P., López-Blanco, E., Marushchak, M., Mastepanov, M., Merbold, L., Parmentier, F.-J., Peichl, M., Sachs, T., Sonnentag, O., Ueyama, M., Voigt, C., Aurela, M., Boike, J., Celis, G., Chae, N., Christensen, T. R., Bret-Harte, M., Dengel, S., Dolman, H., Edgar, C., Elberling, B., Euskirchen, E., Grelle, A., Hatakka, J., Humphreys, E., Järveoja, J., Kotani, A., Kutzbach, L., Laurila, T., Lohila, A., Mammarella, I., Matsuura, Y., Meyer, G., Nilsson, M., Oberbauer, S., Park, S.-J., Petrov, R., Prokushkin, A., Schulze, C., St. Louis, V., Tuittila, E.-S., Tuovinen, J.-P., Quinton, W., Varlagin, A., Zona, D., and Zyryanov, V.: The ABCflux database: Arctic-boreal CO₂ flux observations and ancillary information aggregated to monthly time steps across terrestrial ecosystems. *Earth Syst. Sci. Data*, 14(1), 179-208, doi: 10.5194/essd-14-179-2022, 2022.
- 940



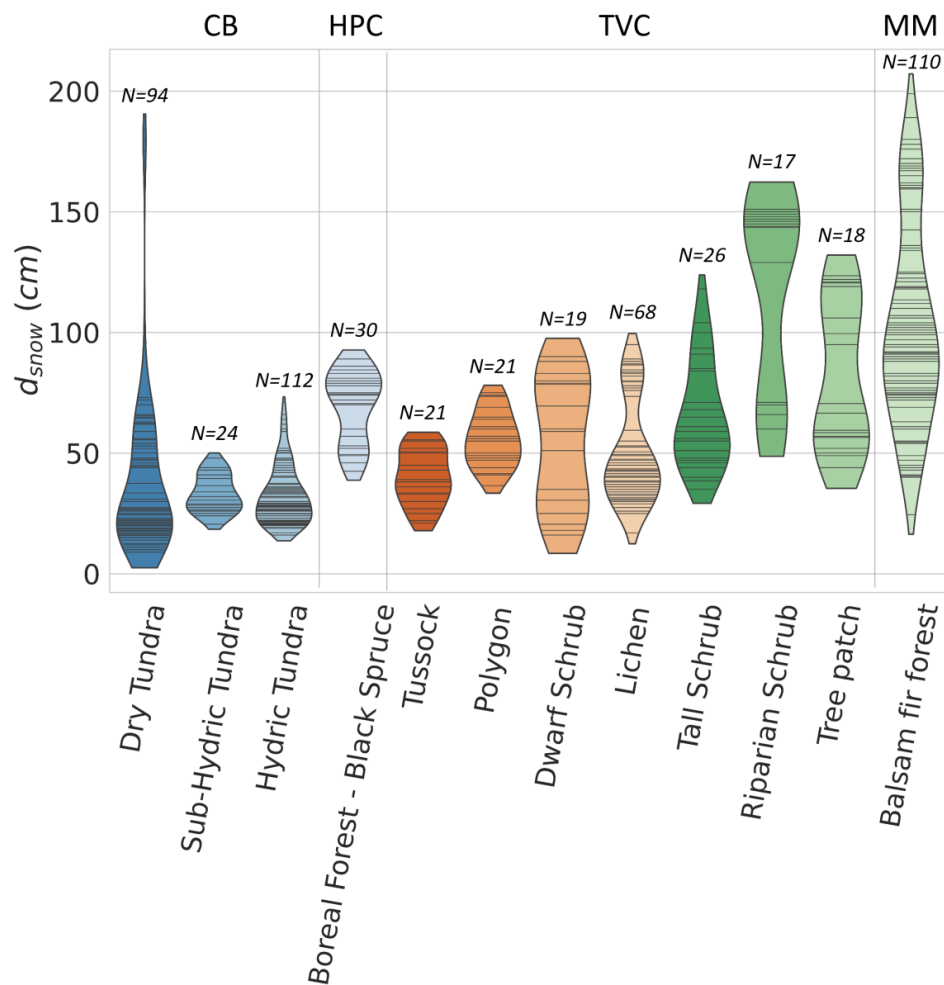
- 945 Virtanen, T. and Ek, M.: The fragmented nature of tundra landscape. *Int. J. Appl. Earth Obs. Geoinf.*, 27(A), 4-12, doi: 10.1016/j.jag.2013.05.010, 2014.
- 950 Wang, T., Ciais, P., Piao, S., Ottlé, C., Brender, P., Maignan, F., Arain, A., Cescatti, A., Gianelle, D., Gough, C., Gu, L., Lafleur, P., Laurila, T., Marcolla, B., Margolis, H., Montagnani, L., Moors, E., Saigusa, N., Vesala, T., Wohlfahrt, G., Koven, C., Black, A., Dellwik, E., Don, A., Hollinger, D., Knohl, A., Monson, R., Munger, J., Suyker, A., Varlagin, A., and Verma, S.: Controls on winter ecosystem respiration in temperate and boreal ecosystems. *Biogeosciences*, 8(7), 2009–2025, doi: 10.5194/bg-8-2009-2011, 2011.
- 955 Wieder, W., Sulman, B., Hartman, M., Koven, C., and Bardford, M.: Arctic Soil Governs Whether Climate Change Drives Global Losses or Gains in Soil Carbon. *Geophys. Res. Lett.*, 46(24), 14486-14495, doi: 10.1029/2019GL085543, 2019.
- 960 Wilcox, E.J., Keim, D., de Jong, T., Walker, B., Sonnentag, O., Sniderhan, A.E., Mann, P. and Marsh, P.: Tundra shrub expansion may amplify permafrost thaw by advancing snowmelt timing. *Arct. Sci.*, 5(4), 202-217, doi: 0.1139/as-2018-0028, 2019.
- 965 Webb, E., Schuur, E., Natali, S., Oken, K., Bracho, R., Krapek, J., Risk, D., and Nickerson, N.: Increased wintertime CO₂ loss as a result of sustained tundra warming. *J. Geophys. Res. Biogeosci.*, 121(2), 249-265, doi: 10.1002/2014JG002795, 2016.
- 970 Yi, Y., Kimball, J., Rawlins, M., Moghaddam, M., and Euskirchen, E.: The role of snow cover affecting boreal-arctic soil freeze–thaw and carbon dynamics. *Biogeosciences*, 12(19), 5811-5829, doi: 10.5194/bg-12-5811-2015, 2015.
- 975 Yi, Y., Kimball, J., Chen, R., Moghaddam, M., and Miller, C.: Sensitivity of active-layer freezing process to snow cover in Arctic Alaska. *Cryosphere*, 13(1), 197-218, doi: 10.5194/tc-13-197-2019, 2019.
- 980 Yli-Halla, M., Lötjönen, T., Kekkonen, J., Virtanen, S., Marttila, H., Liimatainen, M., Saari, M., Mikkola, J., Suomela, R., and Joki-Tokola, E.: Thickness of peat influences the leaching of substances and greenhouse gas emissions from a cultivated organic soil. *Sci. Total Environ.*, 806(1), 150499, doi: 10.1016/j.scitotenv.2021.150499, 2022.
- 980 Zhang, L., Zhao, T., Jiang, L., and Zhao, K.: Estimate of Phase Transition Water Content in Freeze–Thaw Process Using Microwave Radiometer. *IEEE Trans. Geosci. Remote Sens.*, 48(12), 4248-4255, doi: 10.1109/TGRS.2010.2051158, 2010.
- 980 Zhu, C., Nakayama, M., and Inouey, H. Y.: Continuous measurement of CO₂ flux through the snowpack in a dwarf bamboo ecosystem on Rishiri Island, Hokkaido, Japan. *Polar Sci.*, 8(3), 218-231, doi: 10.1016/j.polar.2014.04.003, 2014.



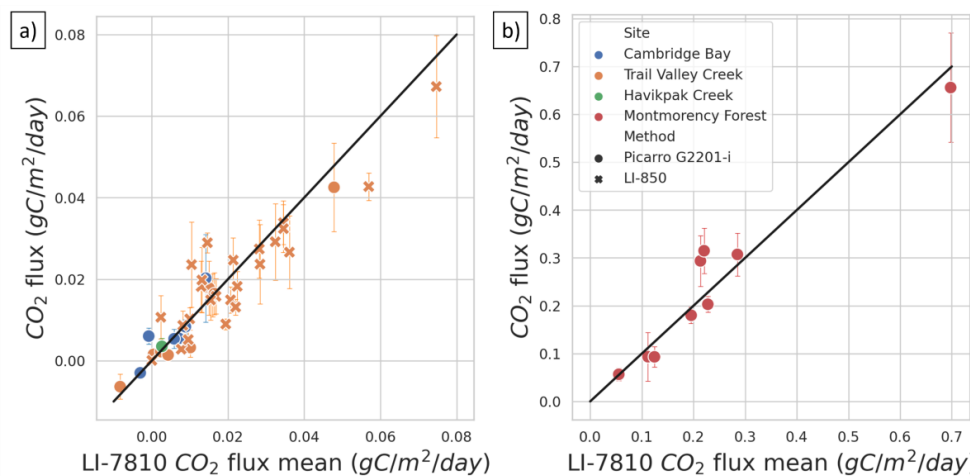
Appendix A

985 **Table A1: Uncertainty sources on F_{CO_2} and their uncertainty. $[CO_2]$ precision was evaluated at a concentration of 400 ppm.**

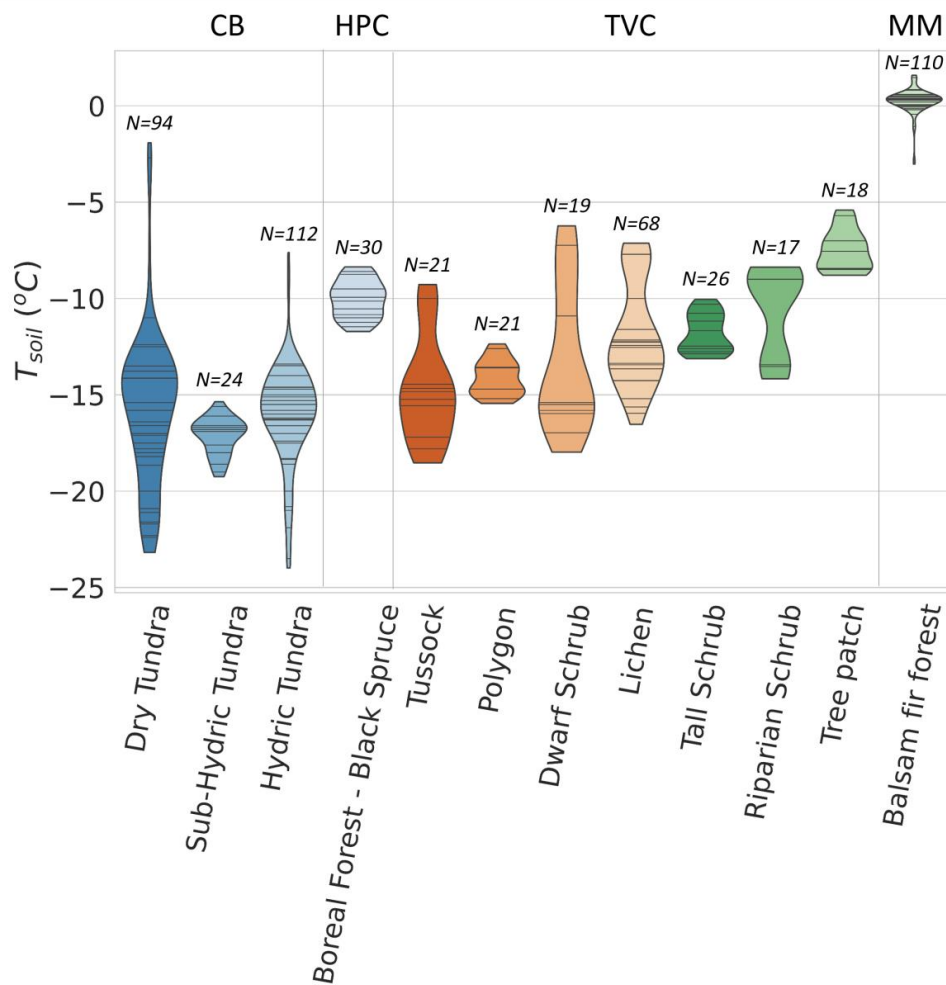
F_{CO_2} uncertainty source	Uncertainty
[CO_2] estimate	
· LI-7810 precision	3,52 ppm (0.88%)
· Measurement stability	3.6 ppm (0.09 %; N=169)
· Reference gas	4 ppm (1 %)
· Calibration fit	3.04 ppm (0.76 %; N=6; $\sigma = 0.15$)
· Transfer, transport and storage test	4.44 ppm (1.11 %; N=6)
Snow density (kg/m^3)	9 %
$d[CO_2]/dz$ linear regression (gC/m^4)	19.4 %



990 **Figure A1:** Violin plot of the snow depth range of sites where F_{CO_2} was estimated. The black stripes inside the violins represent data point. CB sites are ordered by increasing hygricity and TVC sites are ordered by increasing soil surface temperature in March 2021 and 2022.



995 **Figure A2:** Comparison of non-growing season CO₂ flux calculated from CO₂ concentration estimated with different gas analyzers. The LI-7810 gas analyzer was used as the reference and is compared to a Picarro G2201-*i* and LI-850. In the arctic biome (a), the correlation coefficient is 0.924 for the Picarro and 0.821 for the LI-850. In the boreal biome (b), the correlation coefficient is 0.929 for the Picarro.



1000 **Figure A3:** Violin plot of the soil temperature (T_{soil}) range of sites where F_{CO_2} was estimated. The black stripes inside the violins represent data point. CB sites are ordered by increasing hygricity and TVC sites are ordered by increasing soil surface temperature in March 2021 and 2022.